Biogeosciences, 15, 2231–2249, 2018
https://doi.org/10.5194/bg-15-2231-2018
© Author(s) 2018. This work is distributed under
the Creative Commons Attribution 4.0 License.

Biogeosciences
Open Access
EGU

Contribution of fine tree roots to the silicon cycle in a temperate forest ecosystem developed on three soil types

Marie-Pierre Turpault[1], **Christophe Calvaruso**[2], **Gil Kirchen**[1], **Paul-Olivier Redon**[3], **and Carine Cochet**[1]

[1]UR 1138, INRA "Biogéochimie des Ecosystèmes Forestiers", Centre INRA de Nancy, Champenoux, 54280, France
[2]EcoSustain, Environmental Engineering Office, Research and Development, Kanfen, 57330, France
[3]Andra, Direction de la Recherche et Développement, Centre de Meuse/Haute-Marne,
Route départementale 960, Bure, 55290, France

Correspondence: Marie-Pierre Turpault (marie-pierre.turpault@inra.fr)

Received: 2 November 2017 – Discussion started: 27 November 2017
Revised: 18 March 2018 – Accepted: 23 March 2018 – Published: 17 April 2018

Abstract. The role of forest vegetation in the silicon (Si) cycle has been widely examined. However, to date, little is known about the specific role of fine roots. The main objective of our study was to assess the influence of fine roots on the Si cycle in a temperate forest in north-eastern France. Silicon pools and fluxes in vegetal solid and solution phases were quantified within each ecosystem compartment, i.e. in the atmosphere, above-ground and below-ground tree tissues, forest floor and different soil layers, on three plots, each with different soil types, i.e. Dystric Cambisol (DC), Eutric Cambisol (EC) and Rendzic Leptosol (RL). In this study, we took advantage of a natural soil gradient, from shallow calcic soil to deep moderately acidic soil, with similar climates, atmospheric depositions, species compositions and management. Soil solutions were measured monthly for 4 years to study the seasonal dynamics of Si fluxes. A budget of dissolved Si (DSi) was also determined for the forest floor and soil layers. Our study highlighted the major role of fine roots in the Si cycle in forest ecosystems for all soil types. Due to the abundance of fine roots mainly in the superficial soil layers, their high Si concentration (equivalent to that of leaves and 2 orders higher than that of coarse roots) and their rapid turnover rate (approximately 1 year), the mean annual Si fluxes in fine roots in the three plots were 68 and 110 $kg\,ha^{-1}\,yr^{-1}$ for the RL and the DC, respectively. The turnover rates of fine roots and leaves were approximately 71 and 28 % of the total Si taken up by trees each year, demonstrating the importance of biological recycling in the Si cycle in forests. Less than 1 % of the Si taken up by trees each year accumulated in the perennial tissues. This study also demonstrated the influence of soil type on the concentration of Si in the annual tissues and therefore on the Si fluxes in forests. The concentrations of Si in leaves and fine roots were approximately 1.5–2.0 times higher in the Si-rich DC compared to the Si-poor RL. In terms of the DSi budget, DSi production was large in the three plots in the forest floor (9.9 to 12.7 $kg\,ha^{-1}\,yr^{-1}$), as well as in the superficial soil layer (5.3 to 14.5 $kg\,ha^{-1}\,yr^{-1}$), and decreased with soil depth. An immobilization of DSi was even observed at 90 cm depth in plot DC ($-1.7\,kg\,ha^{-1}\,yr^{-1}$). The amount of Si leached from the soil profile was relatively low compared to the annual uptake by trees (13 % in plot DC to 29 % in plot RL). The monthly measurements demonstrated that the seasonal dynamics of the DSi budget were mainly linked to biological activity. Notably, the peak of dissolved Si production in the superficial soil layer occurred during winter and probably resulted from fine-root decomposition. Our study reveals that biological processes, particularly those involving fine roots, play a predominant role in the Si cycle in temperate forest ecosystems, while the geochemical processes appear to be limited.

1 Introduction

It has recently been shown that intense biogeochemical cycling of Si occurs in the different terrestrial ecosystems, i.e. wetlands (Struyf et al., 2007; Emsens et al., 2016), grasslands (Blecker et al., 2006; White et al., 2012), tropical forests (Lucas et al., 1993; Alexandre et al., 1997, 2011) and tem-

perate forests (Bartoli, 1983; Watteau and Villemin, 2001; Gérard et al., 2008; Cornelis et al., 2010a, 2011; Sommer et al., 2006, 2013). Several review papers described how dissolved Si (DSi) in soil is taken up by vascular plants and translocated into biogenic Si (BSi) in an opal form, which is deposited into the cell walls, cell luminas and intercellular spaces (Jones and Handreck, 1965; Conley, 2002; Cornelis et al., 2010b; Struyf and Conley, 2012). These structures are called phytoliths. Other important producers of BSi are sponges and protists (diatoms, testate amoebae) (Struyf and Conley, 2012; Sommer et al., 2006; Puppe et al., 2014, 2015). In terrestrial ecosystems BSi pools can be separated into phytogenic (phytoliths), microbial and protozoic pools. The latter is represented in soils by idiosomic testate amoebae (Puppe et al., 2014).

According to Conley (2002), the annual fixation of DSi in terrestrial ecosystems has been estimated to range from 60 to 200 Tmoles. That represents 10 to 40 times more than yearly exported DSi and suspended BSi from the terrestrial geobiosphere to the coastal zone (Conley, 2002). Vegetation can thus be considered a product of BSi which returns to the soil as organic matter through biological recycling. Because BSi in general is more soluble than silicate minerals, BSi strongly contributes to the DSi pool (Fraysse et al., 2009; Cornelis and Delvaux, 2016).

Based on the assumption that the storage of Si is limited in roots (Bartoli and Souchier, 1978) and because fine-root sampling and cleaning before analyses are long and tedious processes, studies in forest ecosystems mainly focus on the importance of litterfall recycling in the Si biogeochemical cycle without quantifying Si in the roots (Gérard et al., 2008; Cornelis et al., 2010a; Sommer et al., 2013).

However, Krieger et al. (2017) recently showed that Si in deciduous trees (European beech, *Fagus sylvatica* and sycamore, *Acer pseudoplatanus*) generally precipitates as a thin layer (< 0.5 µm) around the cells, especially in roots and bark. These small-scale phytogenic Si were demonstrated to influence various soil and plant processes (Meunier et al., 2017; Puppe et al., 2017). Maguire et al. (2017), who examined the impact of climate change on Si uptake by trees, observed that fine roots of sugar maple (*Acer saccharum*), which represented only 4 % of the tree's biomass, accumulated 29 % of the Si.

Considering the high Si content of fine roots (Krieger et al., 2017; Maguire et al., 2017) and their rapid turnover in forest ecosystems (approximately 1 year in beech forests in Europe; Brunner et al., 2013), we hypothesized that fine roots could significantly contribute to the input of BSi into the soil.

To test this hypothesis, during a 4-year observation period we quantified (i) the total and annual accumulations of Si in stand below-ground and above-ground biomasses while distinguishing annual and perennial compartments, and (ii) the Si input fluxes in the forest floor (litterfall and small woods, above-ground exploitation residues) and in the soil (fine roots and below-ground exploitation residues). The study took place in a lowland (low lateral transfer of material) deciduous temperate forest developed on three soils, ranging from a shallow calcic soil to a deep acidic soil, with mull to acid mull humus. These humus forms quickly degrade and contain few soil particles and no roots, thus allowing determination of the DSi issued from the degradation of organic layers contrary to mor or moder humus forms (Sommer et al., 2006; Cornelis et al., 2010a). In addition, we quantified the DSi inputs and outputs in these ecosystems monthly, i.e. rainfall, foliar leaching and drainage, in order to assess the seasonal dynamics of these fluxes induced by biological activities.

2 Materials and methods

2.1 Experimental site

The experimental site, hereafter referred to as the Montiers site (http://www.nancy.inra.fr/en/Outils-et-Ressources/montiers-ecosystem-research, last access: 12 April 2018), is located in the Montiers-sur-Saulx beech forest in northeastern France (Meuse, France, latitude 48°31′54″ N, longitude 5°16′08″ E). The site is 73 ha and has been managed jointly by the INRA-BEF (French National Institute for Agricultural Research – Biogeochemical cycles in Forest Ecosystems research unit) and by the ANDRA (French National Radioactive Waste Management Agency) since 2012. The different steps of site establishment are described in detail in Calvaruso et al. (2017). The Montiers site is part of different national and international research networks, i.e. SOERE-OPE (Long-lasting observation and experimentation for the research on environment – Perennial Environment Observatory; http://www.andra.fr/ope/index.php?lang=en&Itemid=127, last access: 12 April 2018) and F-ORE-T (Functioning of Forest Ecosystems; http://www.gip-ecofor.org/f-ore-t/, last access: 12 April 2018), and AnaEE (Analysis and Experimentations on Ecosystems; https://www.anaee.com/, last access: 12 April 2018). The mean annual rainfall and temperature over the last 20 years were 1069 mm and 9.8 °C, (calculated from Météo-France data). The geology of the Montiers site consists of two overlapping soil parent materials: an underlying Tithonian limestone surmounted by detrital acidic Valanginian sediments. The calcareous bedrock mainly contains calcium carbonate and ~ 3.4 % clay minerals. The overlying detrital sediments are complex, as they result from various depositions and are composed of silt, clay, coarse sand and iron oxide nodules (for more details, see Calvaruso et al., 2017). The site is covered by a homogeneous stand of the same age (approximately 50 years old in 2010) with the same management approaches. The stand was mainly composed of beech (89 %) and 11 % of other deciduous species, i.e. sycamore maple (*Acer pseudoplatanus*), ash (*Fraxinus excelsior*), pedunculate oak (*Quercus robur* L.), European hornbeam (*Carpinus betulus* L.) and wild cherry

Table 1. Physicochemical properties of the three studied soils at the Montiers site (plot DC, plot EC, plot RL). Presented are the mean values for bulk density (BD), textural distribution (clay, fine silt, coarse silt, fine sand and coarse sand), total rock volume (RV), soil water holding capacity (SWHC), soil water pH (pH_w), organic matter content (OM), cation exchange capacity (CEC; $cmol^+ kg^{-1}$) and base-cation saturation ratio (S/CEC, with S as the sum of base cations). SD values are given in italics. Table adapted from Kirchen et al. (2017).

	Depth	BD	Clay	Fine silt	Coarse silt	Fine sand	Coarse sand	RV	SWHC	pH_w	OM	CEC	S/CEC
	(cm)	($g\,cm^{-3}$)			($g\,kg^{-1}$)			(%)	(mm)		($g\,kg^{-1}$)	($c\,mol^+\,kg^{-1}$)	(%)
Dystric Cambisol	0–5	0.98	255	281	160	185	121	1.4	8.2	4.9	68	6.7	64.2
		0.12	*25*	*24*	*17*	*36*	*19*				*22*	*3.0*	*23.4*
	5–15	0.94	245	276	162	184	131	1.4	16.5	4.8	43	4.2	35.0
		0.17	*26*	*29*	*17*	*40*	*24*				*16*	*2.2*	*20.9*
	15–30	1.23	268	280	161	170	115	1.8	22.7	4.8	26	3.5	25.9
		0.22	*28*	*31*	*21*	*44*	*31*				*9*	*0.9*	*14.1*
	30–45	1.36	306	262	150	161	119	2.3	22.6	4.9	15	4.3	36.2
		0.18	*65*	*45*	*27*	*47*	*32*				*5*	*1.6*	*15.8*
	45–60	1.45	355	229	126	166	141	3.6	18.1	5.1	10	5.7	55.1
		0.15	*100*	*45*	*31*	*49*	*39*				*2*	*2.6*	*21.9*
Eutric Cambisol	0–5	1.03	242	242	143	290	83	2.3	9.2	5.4	73	10.1	83.3
		0.11	*52*	*16*	*13*	*36*	*24*				*26*	*5.4*	*14.2*
	5–15	0.93	241	246	145	287	82	3.1	18.2	5.2	45	7.8	59.1
		0.13	*65*	*17*	*13*	*45*	*24*				*29*	*7.3*	*23.6*
	15–30	1.23	294	234	136	273	64	7.6	19.1	5.3	27	7.7	60.9
		0.19	*83*	*23*	*17*	*55*	*11*				*13*	*3.9*	*23.3*
	30–45	1.35	420	188	107	214	71	29.0	14.7	5.3	17	13.2	68.4
		0.18	*141*	*43*	*31*	*63*	*20*				*8*	*6.9*	*27.2*
	45–60	1.32	523	154	85	176	63	40.3	10.3	5.4	11	17.8	75.6
		0.23	*136*	*42*	*32*	*57*	*31*				*4*	*8.8*	*17.4*
Rendzic Leptosol	0–5	0.88	449	227	123	119	41	2.3	9.8	5.7	109	24.9	97.8
		0.14	*80*	*54*	*26*	*39*	*15*				*27*	*8.3*	*5.4*
	5–15	0.98	430	224	114	123	59	4.9	19.2	5.7	71	20.0	94.2
		0.12	*82*	*56*	*36*	*37*	*21*				*23*	*7.9*	*6.6*
	15–30	1.06	516	169	77	102	63	36.4	12.5	6.0	42	23.2	99.3
		0.22	*81*	*50*	*38*	*42*	*24*				*10*	*6.4*	*5.3*

(*Prunus avium*). The site is also composed of three different soil types, i.e. Dystric Cambisol (DC), Eutric Cambisol (EC) and Rendzic Leptosol (RL) (FAO, 2016). A schematic representation of the soil profiles and their locations are presented in Kirchen et al. (2017). Table 1 presents the main characteristics of these different soil types, ranging from acidic and deep soils to calcic and superficial soils, developed on acidic Valanginian and detritic sediments and Portlandian limestone, respectively. Humus type is a eutrophic mull for the RL and EC and an acidic mull for the DC.

Three experimental plots, with an area of 1 ha each, were built on the three different soils to monitor water and element fluxes as well as tree growth over 4 years. Each plot was subdivided into four subplots (replicates) of which three were equipped with the same monitoring devices designed for the sampling of above-ground and below-ground solutions at different depths, soil at different depths, organic horizons and litterfall, and four were equipped with devices for standing above-ground and below-ground biomasses as well as tree growth. In addition, a 45 m high flux tower was placed within the site (close to plot DC) to collect rainfall and atmospheric deposits.

2.2 Sampling

2.2.1 Solutions and dust deposits

Solutions and dust deposits were sampled every 4 weeks between January 2012 and December 2015, representing 4 years of monitoring.

Rainfall was collected on top of the flux tower in three polyethylene collectors (0.24 m^2 opening) to obtain dust deposition. The procedure of dust deposit sampling is described in Lequy et al. (2014). Briefly, rainfall was centrifuged for 40 min at 3500 $tr\,min^{-1}$ to separate the solid phase from the solution (the solid phase consisting of the dust deposits). Rainfall volumes were obtained from a Météo-France weather station located in Biencourt-sur-Orge (Meuse, France), which is 4.3 km from the Montiers site.

The throughfall was collected in each replicate by 4 polyethylene gutters (0.39 m^2 opening), placed 1.2 m above the forest ground.

The stemflow was collected in each replicate on six trees of different sizes using polyethylene collars attached horizontally to the stem at 1.50 m. Trees were chosen to cover most of the range of stem circumferences at 130 cm height (C130) in each plot. To prevent the solution from freezing, the stemflow was collected in underground storage containers during the winter.

The gravitational soil solutions (zero-tension lysimeters, ZTL) were collected beneath the forest floor and at different soil depths, −10 and −30 cm (in DC, EC and RL), −60 cm (in DC and EC) and −90 cm (in DC), with large plate lysimeters (40 cm × 30 cm, 0.12 m^2; 3 repetitions per soil depth and per replicate) or thin rod-like lysimeters (0.07 m^2; in clusters of 8; 3 repetitions per soil depth and per replicate).

The bound soil solutions (tension lysimeters, TL) were collected with ceramic cups inserted into the soil at different depths, −10 and −30 cm (in DC, EC and RL), −60 cm (in DC and EC) and −90 cm (in DC), with four repetitions per depth and per replicate. These ceramic cups were connected to an electric vacuum pump that maintained a constant depression between −0.5 and −0.6 bar.

2.2.2 Tree compartments

Three beech trees were harvested in each plot in 2009 to collect stem wood, stem bark and branches. Subsequently, the branches were separated into different classes, i.e. < 4, 4–7 and > 7 cm in diameter, according to Henry et al. (2011). The detailed procedure for collecting stem wood, stem bark and branches is described in Calvaruso et al. (2017).

The fine roots (< 2 mm diameter) were collected during March–April 2011 in three soil pits (approximately 0.4 m wide) for each replicate, where the soil material was cut and extracted by layer (0–5, 5–15, 15–30, 30–45, 45–60 and 60–90 cm, when possible). A two-step procedure was applied to accurately assess the fine-root biomass (Bakker et al., 2008), without having to transport the soil to the laboratory. The first step involved collecting, in situ, the fine roots from the block of soil extracted from each soil layer. Then, a part of the soil block (approximately 2 kg) was collected. The second step, at the laboratory, consisted of using a tweezer to collect all the remaining fine roots in this soil aliquot. This second step allowed for the assessment of the fraction of fine roots uncollected during the first step. The fine roots collected during the two steps were washed at the laboratory, dried in a stream air drier for 3 days and then weighed. For each layer, the total biomass of fine roots was obtained by summing the fine-root biomass collected during the first step and the fine-root biomass collected during the second step and was multiplied by the ratio of total soil block mass/soil aliquot mass. Roots with a diameter > 2 cm (small and coarse roots) were collected in February 2017 in three soil pits (approximately 0.4 m wide) for each plot where soil material was cut and extracted at approximately 20 cm depth. This method does not allow quantification of small- and coarse-root biomass, which were determined through allometric equations (Le Goff and Ottorini, 2001). An aliquot of each root sample (fine, small and coarse) was then collected to determine element concentration. Each aliquot was carefully washed under a binocular microscope with distilled water, using tweezers and an ultrasound gun. The absence of soil particles was carefully checked on each root sample under a binocular microscope with a magnification of 10×. The operation was repeated until all soil particles were removed to prevent soil pollution in the root analyses. A second check using a scanning electron microscope (SEM) equipped with an energy-dispersive X-ray spectrometer (EDX) was carried out on 12 randomly selected subsamples of fine roots by plot (for more details, see Sect. 2.3.4). All observed subsamples were free from soil particles.

The litterfall was collected in six litter traps (0.34 m^2 each) per replicate. The litter was harvested seven times per year, avoiding litter degradation in the litter traps. During the harvest, the litter was separated into three compartments, i.e. (i) leaves, (ii) buds, beechnuts and fruit capsules as well as (iii) small branches falling from the trees. The leaves, buds, beechnuts and fruit capsules belong to annual tree compartments (recycling each year), while small branches belong to perennial compartments.

2.2.3 Forest floor

We defined the forest floor by the set of organic horizons (Oln, Olv, Of and Oh) above the organo-mineral horizon (Ah) and the small dead wood at the soil surface.

Organic horizons were collected in June 2010 in a calibrated metal frame (surface area of 0.1 m^2). Nine samples were collected in each replicate. Because the lower organic horizons were in direct contact with the superficial soil layer, it was very difficult to sample them without soil contamination. The presence of soil particles, very rich in Si, mixed with the organic horizons, can induce a drastic overestimation of the Si pool in this compartment. As a result, we decided to carefully sample, on site, six organic horizon samples without the fraction contacting the soil, called "pure organic horizons". These pure organic horizons were used to determine the soil fraction in the organic horizon collected on the three plots (see the method in Sect. 2.4.2).

Small dead wood from the previous thinning (winter 2009–2010) was harvested in June 2010 at the three plots in a calibrated metal frame (surface area of 0.6084 m^2). Nine samples were collected in each replicate, according to a grid.

2.2.4 Soil

Nine soil samples were collected in June 2010 in each replicate, along a 15 m × 15 m grid. At each point, samples were

extracted through an auger by layers 0–5, 5–15, 15–30, 30–45, 45–60 and 60–90 cm, when possible.

2.3 Analytical methods

2.3.1 Si content in solutions

Solutions of rainwater, stemflow, throughfall, forest floor and soil were filtered at 0.45 µm, stored at 4 °C and analysed during the week following the sampling. The Si content in the solutions was measured by inductively coupled plasma-atomic emission spectrometry (ICP-AES Agilent Technologies 700 type ICP-OES, Santa Clara, USA).

2.3.2 Si content in biomass

Samples from the above-ground and below-ground compartments of the trees, litterfall and forest floor were dried in a stream air-drier (at 65 °C), then ground and encapsulated for analysis. The total Si content in the biomass was assessed by X fluorescence using an X fluorescence sequential spectrometer S8 TIGER 1 kW (Bruker, Marne la vallée, France).

2.3.3 Si content in soil and dust deposits

The total Si content in soil organo-mineral and mineral layers (preliminarily sieved at 2 mm) and in dust deposits was determined by inductively coupled plasma-atomic emission spectrometry (700 Series ICP-OES, AGILENT TECHNOLOGIES) after alkaline fusion in $LiBO_2$ and in HNO_3.

2.3.4 Microscopic analysis

Between 9 and 12 randomly selected samples of fine roots, stem and branch bark, fruit capsules, bud scales and fresh and altered leaves (from organic horizons) collected on beech trees for each plot were mounted on glass plates using double-coated carbon conductive tabs and covered with carbon. These samples were examined at the GeoRessources laboratory (University of Lorraine) for biomineral occurrence and composition using a Hitachi S-4800 SEM equipped with an EDX and containing a lithium-drifted Si detector. The SEM analyses were carried out using an acceleration voltage of 10 or 15 kV.

2.4 Calculation of Si pools and fluxes in solutions and solids

In each plot, Si fluxes and pools were obtained by multiplying the amount of solution or solid by the concentration of Si in the given compartment. All monthly Si fluxes were calculated on a 1 ha basis and were summed over calendar years to compute the annual fluxes. The DSi budget was also calculated for forest floor and soil layers using the difference between input and output fluxes.

In the following sections (2.4.1 to 2.4.10), we will only present the Si fluxes or pools for which the method of calculation differs from that of the calculation of multiplying the amount of solution or solid by the concentration of Si in the compartment.

2.4.1 Dust deposits

To take into account the loss of particles during the collection of dust deposits from rainfall, a test using standard minerals was done to assess the efficiency of the procedure (Lequy et al., 2014). The efficiency was estimated at 72 %. Thus, the total weight of dust deposits per year was determined as the weight of dust deposits collected on site, divided by a correction factor of 0.72.

2.4.2 Organic horizons

The percentage of soil mixed with the organic horizons was determined through the use of titanium (Ti). This element is a good tracer of soil pollution in the collected organic horizons because Ti is in very low abundance in pure organic horizons ($< 0.3\,mg\,kg^{-1}$), but more abundant in soils ($> 4\,mg\,kg^{-1}$). We measured Ti content in the soil surface layer (0–5 cm), in the pure organic horizons and in the organic horizons collected on the three plots. The percentage of soil in the organic horizons was calculated using Eq. (1):

$$\text{Soil } \% = [(Ti_{Hb} - Ti_{Hp})/(Ti_S - Ti_{Hp})], \quad (1)$$

where Ti_{Hb} is the concentration of Ti in the organic horizons, Ti_{Hp} is the concentration of Ti in the pure organic horizons, and Ti_S is the mean concentration of Ti in the 0–5 cm horizon of soil for each plot. The mean soil fraction represented less than 5% of the total organic horizon mass in our study. The fraction of Si introduced by soil contamination was deducted to obtain the Si content in the organic horizons.

2.4.3 Stemflow and stand deposition

To transform the stemflow volumes into a water flux, C130 was assumed to explain the stemflow volume variability between individuals within a species. Thus, all the trees in each plot were separated into several C130 classes, and the correlation between the stemflow volume and the C130 was verified for the entire sampling period. Using a trend line equation, a mean monthly stemflow volume was then assigned to each C130 class. The stemflow at the plot scale for a given C130 class (SF_z; in mm) is given by following Eq. (2):

$$SF_z = V_z \cdot \left(\frac{N_z}{A}\right), \quad (2)$$

where z is the C130 class, V_z is the mean stemflow volume per tree in the given C130 class (in L), N_z is the number of trees in the given C130 class and A is the plot area (in m^2). Total stemflow at the plot scale was obtained by summing the stemflow fluxes of all C130 classes.

The Si stand deposition, i.e. the amount of Si ($kg\,ha^{-1}\,yr^{-1}$) reaching the soil after crossing over the canopy, was determined as the sum of the Si fluxes in throughfall and stemflow.

2.4.4 Drainage flux

The BILJOU© model (Granier et al., 1999) was applied in the three plots at the Montiers site to assess the water drainage flux for the different soil layers. The detailed procedure and the data are presented in Kirchen et al. (2017). The gravitational water flux was determined for each soil layer and date from the collected gravitational volume. The bound water flux was obtained by subtracting the water gravitational flux from the modelled water drainage flux. In this study, we determined that the water gravitational flux/water bound flux ratio was approximately 80/20, which is similar to the measurement from a Cl tracer in a beech temperate forest in Fougères (western France) in Legout et al. (2009).

Thus, the monthly drainage fluxes of the elements were calculated at each depth following Eq. (3):

$$D_{Si} = D_G \cdot C_{SiG} + D_B \cdot C_{SiB}, \quad (3)$$

where D_{Si} is the drainage flux of Si, D_G is the water drainage via rapid gravitational transfer, C_{SiG} is the concentration of Si in the gravitational soil solution collected with zero-tension lysimeters, D_B is the water drainage via slow bound transfer, and C_{SiB} is the concentration of Si in the bound soil solution collected in ceramic cups.

The element mass balances were calculated for the following soil layers, according to the installation depths of the lysimeters in the three plots: forest floor, from the forest floor to −10 cm, between −10 and −30 cm, between −30 and −60 cm and between −60 and −90 cm. For each soil layer, the mass balance of the elements was calculated as the difference between the drainage at the bottom of the layer and the drainage entering the layer (Eq. 4):

$$MB_{Si} = D_{Si2} - D_{Si1}, \quad (4)$$

where MB_{Si} is the mass balance of Si in a given soil layer, D_{Si1} is the incoming drainage flux of Si, and D_{Si2} is the drainage flux at the bottom of the soil layer.

2.4.5 Above-ground tree biomass

The evaluation of above-ground tree biomass was calculated according to procedures described in Saint-André et al. (2005). It included four steps: (i) the circumference of all trees was measured at 130 cm height, C_{130}, in autumn 2011 and 2015; (ii) eight trees in each plot, representing the range of C_{130}, stem bark and wood and 0–4, 4–7 and > 7 cm diameter branches were sampled; (iii) the weighed allometric equations fitted for each ecosystem compartment were calculated according to Calvaruso et al. (2017); and (iv) tree biomass (stem bark and wood and 0–4, 4–7 and > 7 cm diameter branches) was quantified per hectare by applying fitted equations to the stand inventories. Annual above-ground biomass production and Si immobilization in above-ground biomass were calculated as the difference between the biomass or Si amount in the biomass calculated for 2015 and 2011, divided by four.

2.4.6 Fine-root flux

The fine-root turnover rate is dependent on the fine-root biomass and the annual production but also on the various methods and calculations used to determine the rate (Jourdan et al., 2008; Gaul et al., 2009; Finer et al., 2011; Yuan and Chen, 2010). In this study, the annual fine-root production was calculated by using the mean fine-root turnover rate of $1.11 \pm 0.21\,y^{-1}$, issued from the last available European data compilation for beech forests (Brunner et al., 2013). The turnover rate corresponds to the ratio between the production of fine roots during the growing season and the mean biomass of living fine roots during the year. The Si flux from fine roots was calculated by multiplying the annual fine-root production by the Si concentration in the fine roots.

2.4.7 Small and coarse roots

The small- and coarse-root biomass as well as the annual root increment were determined using allometric equations, linking the stem diameter at breast level and root biomass of beech trees (Le Goff and Ottorini, 2001).

The pools and fluxes of Si in small and coarse roots were calculated by multiplying the total biomass or the annual root increment by the Si concentration in small and coarse roots.

2.4.8 Exploitation residuals and harvest

To take into account the influence of forestry practices after 2010 on the Si cycle, we simulated a stand thinning based on the forestry practices applied in the Montiers massif by the French National Forestry Office. At this stage of stand development, the National Forestry Office carries out a thinning every 7 years, with an above-ground biomass cut of approximately $40 \times 10^3\,kg\,ha^{-1}$. Because the amount of biomass cut is dependent on the stand above-ground biomass, we integrated this parameter into our calculation of exploitation residuals and harvest.

We determined that the above-ground biomass that will be cut during the next thinning (winter 2017–2018) will be approximately 40.0, 44.3 and $35.0 \times 10^3\,kg\,ha^{-1}$ in plots DC, EC and RL. The root biomass remaining from this thinning will represent approximately 7.9, 9.6 and $6.9 \times 10^3\,kg\,ha^{-1}$ in plots DC, EC and RL.

From the data regarding the proportion of the different tree compartments in the total above-ground biomass at the Montiers site (stem wood and bark, < 4, 4–7 and > 7 cm diameter branches; Calvaruso et al., 2017), we determined the biomass

of residuals (< 4 and 4–7 cm diameter branches) and exports (> 7 cm diameter branches, stem wood and bark) issued from this thinning for each plot. The roots were not exported.

Because thinning in this region is generally done every 7 years, we obtained the annual Si amounts returned to the soil and exported by dividing the total exploitation residuals by seven.

2.4.9 Foliar leaching

The amount of Si released in foliar leachates throughout the year (Si_{FL}, in kg Si ha^{-1} yr^{-1}) was calculated using Eq. (5):

$$Si_{FL} = Si_{SD} - Si_{R}, \quad (5)$$

where Si_{SD} is the amount of Si in the stand deposition throughout the year, and Si_{R} is the amount of Si in annual rainfall. All these parameters were assessed in kg Si ha^{-1} yr^{-1}.

2.4.10 Tree uptake

The amount of Si taken up by trees throughout the year (Si_{Up}, in kg Si ha^{-1} yr^{-1}) was calculated using Eq. (6):

$$Si_{Up} = Si_{IAG} + Si_{IBG} + Si_{RFL}, \quad (6)$$

where Si_{IAG} is the amount of Si immobilized in the total above-ground biomass of trees (stem bark and wood, branches, leaves and buds, beechnuts and fruit capsules) throughout the year, Si_{IBG} is the amount of Si immobilized in the total below-ground biomass of trees (coarse, small and fine roots) throughout the year, and Si_{RFL} is the amount of Si released in foliar leachates throughout the year. All these parameters were assessed in kg Si ha^{-1} yr^{-1}.

2.5 Statistical analysis

The descriptive statistical parameters (e.g. mean, SD, variation coefficient) were performed using XLSTAT 2017 software. The normality of the distribution was checked using the Shapiro–Wilk test. As our data did not follow a normal distribution, the non-parametrical Kruskal–Wallis test was performed to determine the significance of differences in biomass pools and increments, Si content, pools and fluxes for each tree compartment, total Si content and pool in soil, and Si content and fluxes in soil solutions between the three soils, at the threshold level of 0.05. The post hoc Bonferroni correction was used for the pairwise comparison. The non-parametrical Mann–Whitney *U* test was also performed to determine the significance of differences in Si content and Si fluxes between gravitational and bound solutions by soil layer for each soil type, at the threshold level of 0.05.

3 Results

3.1 Si in solids

3.1.1 Microscopic observations of Si deposits in vegetation and the forest floor

In fresh leaves, Si precipitates in cell walls but also in intercellular spaces, generally forming Si deposits called phytoliths, which are several micrometres (Fig. 1a). In all tree compartments except wood, these Si deposits mostly occurred as fine coating layers thinner than 0.3 µm in the inner cell walls of fruit capsules (Fig. 1b), stem bark (Fig. 1d and e), bud scales (Fig. 1f) and roots (Fig. 1g–i). The cells covered with Si deposits were in the external parts of the roots, branches and stem bark (Fig. 1d and g). Occasionally, Si was present on cell lumina (Fig. 1e).

Aged leaves in the organic horizon were colonized by hyphae and amoebae (Fig. 1c) and presented large voids. The Si deposits disappeared from the plant cells but were present in the observed testate amoebae.

3.1.2 Si pools and fluxes in above-ground tree biomass

The calculated standing above-ground biomass in 2011 increased as RL < DC < EC, with significant differences between EC and RL (factor of 1.4) (Table 2). The stem bark had the highest Si concentration in the three plots, and the Si pool in this compartment represented approximately 40 % of the total Si pool in the above-ground tree biomass. The younger the structures were, the higher the Si concentration. Small branches were approximately 3 times more concentrated than coarse branches in the three soils (Table 2). The amount of Si immobilized in the standing above-ground biomass ranged from 20.1 kg ha^{-1} on the RL to 26.2 kg ha^{-1} on the EC. The annual biomass production between 2011 and 2015 increased as RL < EC < DC, with significant differences between DC and RL (factor of 1.7). As a result, the amount of Si immobilized in the above-ground biomass each year between 2011 and 2015 ranged from 0.98 kg ha^{-1} on the RL to 1.82 kg ha^{-1} on the DC.

3.1.3 Si pools and fluxes in below-ground tree biomass

The fine-root biomass measured for the entire soil profile was calculated between 7.3 t ha^{-1} for the DC (90 cm thickness) and 10.6 t ha^{-1} for the EC (90 cm thickness) (Table 2). However, the fine-root density (in t ha^{-1} for one cm of soil) in the RL was higher. Regardless of the soil type, fine-root biomass decreased with depth. No significant difference in fine-root biomass was observed for any soil layer between the three soils. The concentrations of Si in fine roots were high in the three soils and increased as RL < EC < DC. The Si pools in the fine roots were significant, reaching almost 100 kg ha^{-1} in the DC. Based on the turnover rate of fine roots, as determined by Brunner et al. (2013) for beech trees, i.e.

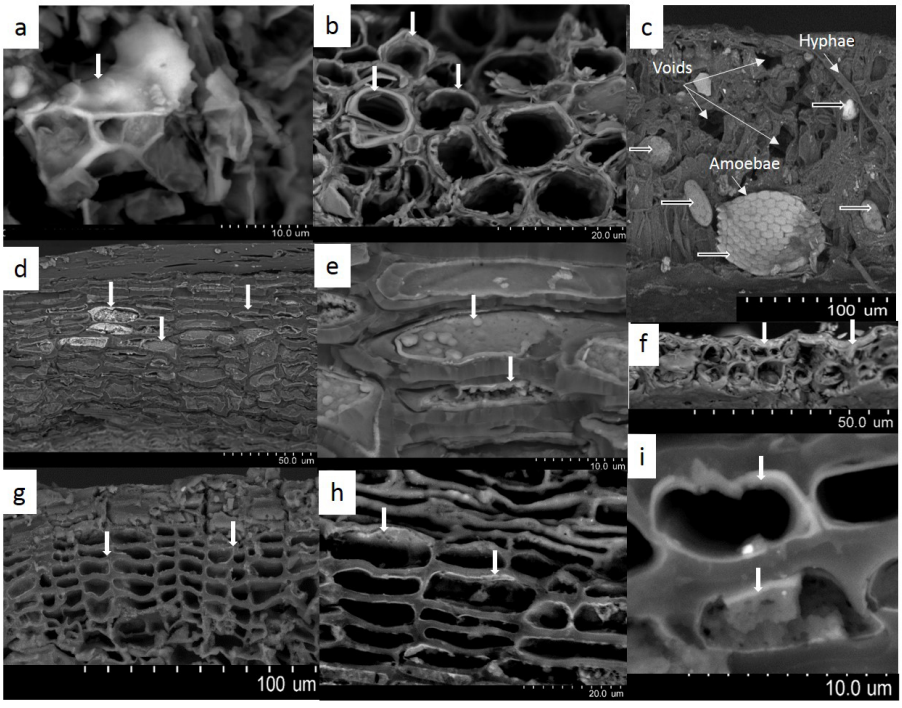

Figure 1. Si in biological tissues of beech trees observed with scanning electron microscopy. **(a)** Si precipitates in the intercellular space of fresh leaves, forming phytoliths (vertical white arrow). Deposits of Si (white arrows) in the inner cell walls of fruit capsules **(b)**, stem bark (**d** and **e**), bud scales **(f)** and roots (**g**, **h** and **i**). **(c)** Hyphae, testate amoebae and large voids in aged litter leaves. Si deposits are only present in the testate amoeba shells (horizontal empty white arrows). The presence of Si was confirmed with EDX (analysed zones indicated by white vertical arrows).

$1.11 \pm 0.21\,y^{-1}$, we calculated that the annual Si fluxes resulting from fine-root decomposition overpassed $100\,kg\,ha^{-1}$ in the DC.

The calculated small- and coarse-root biomass was 3 times higher than that of the fine roots, thus representing approximately 75 % of the total root biomass in the three plots, but the concentrations of Si in coarse roots were 2 orders of magnitude lower than the concentration in fine roots. As observed for fine roots, the Si concentrations in coarse roots were higher in the DC compared to the RL. The annual immobilization of Si in coarse roots was very low for the three soils and was negligible in comparison to the flux induced by fine-root functioning.

3.1.4 Si fluxes in exploitation residues and harvests

The biomass of below-ground and above-ground exploitation residues expressed on an annual basis overpassed $2.0 \times 10^3\,kg\,ha^{-1}\,yr^{-1}$ (Table 2), with a 1 : 1 ratio below-ground / above-ground. The above-ground exploitation residues were 3 to 6 times more concentrated in Si than the below-ground ones. The amount of Si returning to the soil through exploitation residues was lower than $0.50\,kg\,ha^{-1}\,yr^{-1}$. This value was very close to the amount of Si exported from the ecosystem through harvests induced by dynamic forestry practice on the study site.

3.1.5 Si pool in forest floor

In 2010, the forest floor biomass drastically differed between the different soil types, about 2 times more on the DC (acid mull) compared to the RL (eutrophic mull). Part of the small wood (residuals from the previous thinning) was higher in the DC compared to the other two soil types, which made up approximately 40 and 20 % of the total forest floor (Table 2). The Si pools in the forest floor ranged from about $150\,kg\,ha^{-1}$ on the RL to about $250\,kg\,ha^{-1}$ on the DC. Because organic horizons have higher concentrations of Si than small woods, organic horizons represented more than 95 % of the Si pools in the forest floor.

3.1.6 Si fluxes in litterfall

The annual litterfall between 2012 and 2015 ranged from 5.2 and $6.0\,t\,ha^{-1}$ (Table 2). No significant difference was observed between the three plots, regardless of the tree compartment. Dead leaves represented approximately 70 % of the total annual litterfall, while branches and twigs represented 10 %, and buds, beechnuts and fruit capsules represented 20 %. Regardless of the soil type, the Si content of leaves

Table 2. Mean Si contents, pools and fluxes in the biomass of the three soils at the Montiers site. SD values are given in brackets. Values with different letters are significantly different according to a Kruskal–Wallis test at the threshold P value level of 0.05 (soil effect; DC, EC and RL). B + W stands for bark and wood.

Plot	Compartment	Biomass pools ($t DM ha^{-1}$)	Biomass increment ($t DM ha^{-1} yr^{-1}$)	Si content ($g kg^{-1}$)	Si pools ($kg ha^{-1}$)	Si fluxes ($kg ha^{-1} yr^{-1}$)
Dystric Cambisol	Leaves	3.8 (0.4)^{a}	3.8 (0.4)^{a}	11.3 (1.8)^{b}	42.7 (4.3)^{b}	42.7 (4.3)^{b}
	Branches/twigs with bark	0.3 (0.2)^{a}	0.3 (0.2)^{a}	1.1 (0.3)^{a}	0.3 (0.2)^{a}	0.3 (0.2)^{a}
	Buds, beechnuts, fruit capsules	1.1 (1.1)^{a}	1.1 (1.1)^{a}	2.4 (1.0)^{a}	1.8 (0.9)^{a}	1.8 (0.9)^{a}
	Total litterfall	5.2 (1.1)^{a}	5.2 (1.1)^{a}		44.8 (5.1)^{b}	44.8 (5.1)^{b}
	Organic horizons	11.5 (2.0)^{a}		21.4 (1.6)^{a}	246.4 (53.1)^{a}	
	Small wood	7.5 (1.9)^{a}		0.8 (0.3)^{a}	6.5 (3.5)^{a}	
	Forest floor	19.0 (2.7)^{a}			252.9 (53.1)^{a}	
	Stem bark	5.5 (0.7)^{a}	0.5 (0.0)^{b}	1.70 (0.33)^{a}	9.4 (1.2)^{a}	0.65 (0.03)^{b}
	Stem wood	84.8 (11.7)^{ab}	6.4 (0.3)^{b}	0.05 (0.00)^{a}	4.0 (0.5)^{a}	0.30 (0.02)^{a}
	Small branches (B + W)	18.7 (2.5)^{ab}	1.2 (0.1)^{b}	0.40 (0.05)^{a}	7.4 (1.0)^{a}	0.49 (0.03)^{b}
	Medium branches (B + W)	10.2 (1.8)^{ab}	1.1 (0.1)^{b}	0.26 (0.04)^{a}	2.6 (0.5)^{ab}	0.29 (0.02)^{b}
	Coarse branches (B + W)	5.1 (1.1)^{ab}	0.8 (0.1)^{ab}	0.13 (0.04)^{a}	0.7 (0.1)^{ab}	0.10 (0.01)^{b}
	Above-ground biomass	125.8 (17.9)^{ab}	10.0 (0.5)^{b}		24.1 (3.3)^{ab}	1.82 (0.10)^{b}
	Fine roots (0–10 cm)	3.2 (0.8)^{a}	3.5 (0.9)^{a}	12.8 (2.3)^{b}	39.5 (7.5)^{a}	43.9 (8.3) ^{a}
	Fine roots (10–30 cm)	2.9 (1.1)^{a}	3.2 (1.2)^{a}	15.0 (2.3)^{c}	43.9 (6.6)^{b}	48.8 (7.3)^{b}
	Fine roots (30–60 cm)	0.9 (0.6)^{a}	1.0 (0.7)^{a}	12.3	10.5	11.7
	Fine roots (60–90 cm)	0.4 (0.1)^{a}	0.4 (0.1)^{a}	12.7	4.7	5.2
	Total fine roots (0–90 cm)	7.3 (1.8)^{a}	8.0 (2.0)		98.7 (13.5)^{b}	109.5 (15.0)^{b}
	Total coarse roots	24.4 (3.5)^{a}	2.83 (0.47)^{a}	0.11 (0.15)^{a}	2.66 (0.39)^{b}	0.31 (0.05)^{b}
	Exploitation residues AG		1.3	0.33		0.42
	Exploitation residues BG		1.1	0.11 (0.15)^{a}		0.12
	Total exploitation residues		2.4			0.54
	Harvests		4.4	0.16		0.71
Eutric Cambisol	Leaves	4.1 (0.5)^{a}	4.1 (0.5)^{a}	8.9 (1.6)^{ab}	35.4 (2.8)^{ab}	35.4 (2.8)^{ab}
	Branches/twigs with bark	0.6 (0.4)^{a}	0.6 (0.4)^{a}	0.9 (0.2)^{a}	0.4 (0.2)^{a}	0.4 (0.2)^{a}
	Buds, beechnuts, fruit capsules	1.3 (1.1)^{a}	1.3 (1.1)^{a}	3.4 (1.9)^{a}	3.0 (0.5)^{b}	3.0 (0.5)^{b}
	Total litterfall	6.0 (1.1)^{a}	6.0 (1.1)^{a}		38.7 (3.1)^{ab}	38.7 (3.1)^{ab}
	Organic horizons	9.6 (1.4)^{a}		17.6 (0.8)^{a}	174.2 (32.8)^{ab}	
	Small wood	2.6 (1.2)^{a}		1.8 (1.1)^{a}	3.9 (1.3)^{a}	
	Forest floor	12.5 (0.6)^{a}			178.1 (32.6)^{ab}	
	Stem bark	6.1 (0.2)^{a}	0.4 (0.0)^{ab}	1.53 (0.28)^{a}	9.3 (0.3)^{a}	0.39 (0.04)^{a}
	Stem wood	109.9 (3.8)^{b}	5.0 (0.6)^{ab}	0.05 (0.00)^{a}	5.1 (0.2)^{a}	0.23 (0.02)^{a}
	Small branches (B + W)	20.8 (0.7)^{b}	0.8 (0.1)^{ab}	0.38 (0.08)^{a}	7.9 (0.3)^{a}	0.31 (0.04)^{ab}
	Medium branches (B + W)	15.2 (0.6)^{b}	1.0 (0.1)^{ab}	0.23 (0.05)^{a}	3.5 (0.1)^{b}	0.23 (0.02)^{ab}
	Coarse branches (B + W)	9.8 (0.6)^{b}	0.9 (0.1)^{b}	0.10 (0.03)^{a}	1.0 (0.1)^{b}	0.09 (0.01)^{ab}
	Above-ground biomass	164.2 (5.7)^{b}	8.0 (0.9)^{ab}		26.9 (0.9)^{b}	1.25 (0.13)^{ab}
	Fine roots (0–10 cm)	4.6 (2.1)^{a}	5.1 (2.4)^{a}	9.6 (2.9)^{ab}	44.5 (13.9)^{a}	49.4 (15.4)^{a}
	Fine roots (10–30 cm)	4.5 (1.8)^{a}	5.0 (1.9)^{a}	8.2 (1.6)^{b}	37.0 (7.1)^{b}	41.1 (7.8)^{b}
	Fine roots (30–60 cm)	1.2 (0.7)^{a}	1.3 (0.8)^{a}	7.5	8.7	9.7
	Fine roots (60–90 cm)	0.4 (0.1)^{a}	0.5 (0.1)^{a}	–	–	–
	Total fine roots (0–90 cm)	10.6 (4.1)^{a}	11.7 (4.5)		90.2 (20.8)^{b}	100.1 (23.1)^{b}
	Total coarse roots	32.3 (1.2)^{b}	4.08 (0.16)^{b}	0.05 (0.08)^{a}	1.51 (0.05)^{a}	0.19 (0.01)^{a}
	Exploitation residues AG		1.4	0.31		0.43
	Exploitation residues BG		1.4	0.05 (0.08)^{a}		0.06
	Total exploitation residues		2.8			0.50
	Harvests		4.9	0.15		0.72
: Rendzic Leptosol	Leaves	4.0 (0.4)^{a}	4.0 (0.4)^{a}	5.6 (1.3)^{a}	22.2 (3.1)^{a}	22.2 (3.1)^{a}
	Branches/twigs with bark	0.5 (0.3)^{a}	0.5 (0.3)^{a}	0.7 (0.1)^{a}	0.3 (0.2)^{a}	0.3 (0.2)^{a}
	Buds, beechnuts, fruit capsules	1.2 (0.9)^{a}	1.2 (0.9)^{a}	3.2 (1.6)^{a}	2.6 (0.5) ^{ab}	2.6 (0.5)^{ab}
	Total litterfall	5.7 (1.0)^{a}	5.7 (1.0)^{a}		25.2 (3.4)^{a}	25.2 (3.4)^{a}
	Organic horizons	8.8 (1.5)^{a}		16.9 (1.4)^{a}	151.3 (22.6)^{b}	
	Small wood	1.9 (2.4)^{a}		1.3 (0.7)^{a}	4.4 (5.7)^{a}	
	Forest floor	10.9 (2.8)^{a}			154.3 (25.3)^{a}	
	Stem bark	6.8 (0.6)^{a}	0.3 (0.0)^{a}	1.34 (0.27)^{a}	9.1 (0.8)^{a}	0.41 (0.05)^{ab}
	Stem wood	80.1 (8.3)^{a}	3.9 (0.5)^{a}	0.06 (0.03)^{a}	5.0 (0.5)^{a}	0.24 (0.03)^{a}
	Small branches (B + W)	15.0 (1.4)^{a}	0.6 (0.1)^{a}	0.29 (0.04)^{a}	4.3 (0.4)^{a}	0.18 (0.02)^{a}
	Medium branches (B + W)	8.6 (1.4)^{a}	0.6 (0.1)^{a}	0.19 (0.04)^{a}	1.6 (0.3)^{a}	0.11 (0.02)^{a}
	Coarse branches (B + W)	4.6 (1.0)^{a}	0.4 (0.1)^{a}	0.10 (0.03)^{a}	0.5 (0.1)^{a}	0.04 (0.01)^{a}
	Above-ground biomass	115.2 (12.8)^{a}	5.8 (0.8)^{a}		20.5 (2.1)^{a}	0.98 (0.13)^{a}
	Fine roots (0–10 cm)	5.1 (1.4)^{a}	5.6 (1.6)^{a}	7.8 (2.2)^{a}	43.5 (14.1)^{a}	48.3 (15.6)^{a}
	Fine roots (10–30 cm)	3.6 (1.6)^{a}	4.0 (1.8)^{a}	4.9 (0.8)^{a}	17.6 (3.0)^{a}	19.6 (3.3)^{a}
	Fine roots (30–60 cm)	NS	NS	–	–	–
	Fine roots (60–90 cm)	NS	NS	–	–	–
	Total fine roots (0–30 cm)	8.7 (3.0)^{a}	9.6 (3.3)		61.2 (16.0)^{a}	67.9 (17.7)^{a}
	Total coarse roots	26.0 (3.0)^{a}	3.09 (0.44)^{a}	0.06 (0.05)^{a}	1.62 (0.19)^{a}	0.19 (0.03)^{a}
	Exploitation residues AG		1.1	0.24		0.27
	Exploitation residues BG		1.0	0.06 (0.05)^{a}		0.06
	Total exploitation residues		2.1			0.33
	Harvests		3.9	0.15		0.57

was higher than the other litterfall compartments, measuring 9–10 times higher than branches/twigs and 2–5 times higher than buds, beechnuts and fruit capsules. Because of their high biomass and Si concentration compared to the other litterfall compartments, leaves were the main fraction of the Si pool (> 90 %) in the litterfall in the three plots. Litter leaves collected in DC were twice as concentrated in Si than litter leaves collected in RL (11.3 against 5.6 $g\,kg^{-1}$), meaning that the annual Si flux from litterfall was significantly higher on the DC (44.8 $kg\,ha^{-1}$) compared to the RL (25.2 $kg\,ha^{-1}$).

3.1.7 Si pool in soils and flux of dust deposits

The total Si content and pools in the fine earth fraction were significantly lower in the RL compared to the DC and to the EC (Table 3). The total Si pools in the first 90 cm of soil overpassed 2.4×10^6 $kg\,ha^{-1}$ in the DC and EC as opposed to approximately 7.2×10^5 $kg\,ha^{-1}$ in the RL.

The dust deposit annual flux between 2012 and 2015, collected on the flux tower of the DC plot above the canopy represented an annual Si input of approximately 6.0 $kg\,ha^{-1}$ (Table 4).

3.2 Si in solution: DSi

3.2.1 Si flux in above-ground solutions

The mean annual Si concentration in the rainfall was very low (Table 4) compared to stand deposition (Table 4), representing an annual Si flux of approximately 0.2 $kg\,ha^{-1}$. Consequently, the stand deposition and foliar leaching did not significantly differ between the three plots (Table 4). In the three plots, the throughfall solution was enriched in Si (Table 4), and its maximum concentration occurred during the leafed period, especially during the senescence period (Fig. 2). Although the stemflow solution was more concentrated in DSi (Table 4) than the throughfall (Table 4), the throughfall contributed a large amount (up to 85 %) to the Si stand deposition.

3.2.2 Si fluxes in the forest floor

Over the study period (2012–2015), the solution collected under the forest floor was enriched in Si compared to the above-ground one (approximately 1 order of magnitude; Table 4) and was equivalent in the three soil types. The net Si production in the forest floor was highest between September and January and was at a minimum in April, particularly in plot RL (Fig. 3). The mean annual DSi production in the forest floor ranged between 12.4 and 9.5 $kg\,ha^{-1}\,yr^{-1}$ in plots DC and RL (Table 4).

3.2.3 Si fluxes in the soil profile

Regardless of the soil type, the mean annual DSi concentration generally increased with soil depth for both kinds of solutions, except in the deeper soil layers where the Si concentration remained constant (Fig. 4a). The DSi concentrations in the gravitational solution (ZTL) in the 0 to 30 cm soil layers and in the bound-solutions (TL) in the 0–60 cm soil layers increased less than in the forest floor. Regardless of the soil type and depth, the TL solutions were more concentrated in DSi than the ZTL solutions (approximately 1.1 to 1.8 times more; Fig. 4a). No matter the depth and the soil type, DSi concentrations in TL solutions showed seasonal variations, with high concentrations between August and December and low concentrations between February and June, which was not the case for ZTL concentrations (Fig. 4b). The maximum concentration of DSi did not depend on the drainage fluxes (data not shown).

The Si budget revealed a net annual production of DSi in the 0–10 and 10–30 cm layers, respectively ranging from 5.3 $kg\,ha^{-1}\,yr^{-1}$ in plot DC to 14.5 $kg\,ha^{-1}\,yr^{-1}$ in plot RL and from 2.3 $kg\,ha^{-1}\,yr^{-1}$ in plot DC to 5.4 $kg\,ha^{-1}\,yr^{-1}$ in plot EC (Fig. 5). The production of DSi drastically decreased with the depth. In the 60–90 cm layer of plot DC, we even observed a decrease in the amount of DSi (Fig. 5), resulting from its immobilization during the autumn (Fig. 3). In addition, we observed high seasonal variations in the DSi budget, which were more marked in the topsoil layers (Fig. 3). The lowest net production in these horizons was between June and August, while the maximum production rates were observed between September and February.

3.3 Si flux taken up by trees

By adding the amounts of the Si accumulated each year in the different tree compartments, i.e. perennial above-ground biomass, leaves, bud scales, beechnuts and fruit capsules, small and coarse roots, and fine roots and the foliar leachate, we determined that the annual uptake of Si by the stand was approximately 157, 141 and 95 $kg\,ha^{-1}$ in plots DC, EC and RL (Fig. 6).

4 Discussion

4.1 Si accumulation and internal fluxes in trees

Perennial tissues, such as stem, branches and coarse roots, with biomass representing more than 90 % of the total tree biomass, contained between 15 % (plot DC) and 20 % (plot RL) of the Si accumulated in the stand. Annual tissues, such as fine roots and litterfall, contained more than half (from 56 % in plot RL to 58 % in plot DC for fine roots) and about a quarter (from 23 % in plot RL to 26 % in plot DC for litterfall) of the Si contained in the stand. High Si deposition in plant tissues enhances their strength and rigidity but also improves their resistance to plant diseases by stimulating defence reaction mechanisms (Epstein, 1999; Richmond and Sussman, 2003). The high amount of Si that accumulated in fine beech roots resulted not only from a higher Si con-

Table 3. Mean total Si content and pool in the fine earth fraction of the three soils at the Montiers site at different depths. SD values are given in brackets. Values with different letters are significantly different according to a Kruskal–Wallis test at the threshold P value level of 0.05 (soil effect; DC, EC and RL).

Soil type	Compartment	Total Si content ($g\,kg^{-1}$)	Total Si pool ($10^3\,kg\,ha^{-1}$)
Dystric Cambisol	0–10 cm	305 (13)^a	297 (33)^b
	10–30 cm	313 (9)^a	708 (50)^b
	30–60 cm	296 (18)^b	1 301 (422)^b
	60–90 cm	230 (28)^b	858 (80)^c
	Total 0–90 cm		3 164 (487)^b
Eutric Cambisol	0–10 cm	361 (11)^b	411 (30)^c
	10–30 cm	360 (13)^b	791 (127)^b
	30–60 cm	295 (62)^b	871 (290)^b
	60–90 cm	224 (28)^b	348 (117)^b
	Total 0–90 cm		2 421 (410)^b
Rendzic Leptosol	0–10 cm	287 (27)^a	233 (18)^a
	10–30 cm	276 (23)^a	427 (27)^a
	30–60 cm	175 (37)^a	42 (27)^a
	60–90 cm	144 (39)^a	27 (8)^a
	Total 0–90 cm		720 (38)^a

Table 4. Si content and fluxes in the ZTL (zero-tension lysimeter) and TL (tension lysimeter) solutions of the three soils at the Montiers site. SD values are given in brackets. Values with different letters are significantly different according to a Kruskal–Wallis test at the threshold P value level of 0.05 (soil effect; DC, EC and RL).

Plot	Level	Si_{ZTL} concentration ($mg\,L^{-1}$)	Si_{TL} concentration ($mg\,L^{-1}$)	Si fluxes ($kg\,ha^{-1}\,yr^{-1}$)
Dystric Cambisol	Rainfall	0.04 (0.08)		0.2 (0.1)
	Throughfall	0.15 (0.18)^a		1.2 (0.6)^a
	Stemflow	0.38 (0.32)^a		0.1 (0.5)^a
	Stand deposition			1.3 (0.3)^a
	Forest floor	1.7 (0.8)^a		13.7 (2.7)^a
	L-10 cm	2.0 (0.7)^a	2.9 (1.0)^a	19.0 (5.6)^a
	L-30 cm	2.6 (0.4)^a	3.5 (1.1)^a	21.4 (8.3)^a
	L-60 cm	2.6 (0.5)^a	4.1 (1.4)^a	22.4 (9.8)^a
	L-90 cm	2.5 (0.3)	3.7 (0.6)	20.7 (7.4)
Eutric Cambisol	Rainfall	0.04 (0.08)		0.2 (0.1)
	Throughfall	0.16 (0.16)^a		1.2 (0.6)^a
	Stemflow	0.53 (0.38)^a		0.2 (0.6)^a
	Stand deposition			1.4 (0.6)^a
	Forest floor	1.5 (0.6)^a		12.6 (4.2)^a
	L-10 cm	2.1 (0.7)^a	3.2 (1.1)^a	21.6 (4.8)^a
	L-30 cm	3.5 (1.6)^a	4.0 (1.1)^a	25.5 (5.9)^a
	L-60 cm	2.8 (0.6)^a	4.5 (1.1)^a	26.2 (6.6)^a
Rendzic Leptosol	Rainfall	0.04 (0.08)		0.2 (0.1)
	Throughfall	0.13 (0.14)^a		1.0 (0.5)^a
	Stemflow	0.42 (0.41)^a		0.1 (0.4)^a
	Stand deposition			1.2 (0.5)^a
	Forest floor	1.4 (0.8)^a		10.7 (1.4)^a
	L-10 cm	2.1 (1.1)^a	3.8 (1.2)^a	25.2 (9.9)^a
	L-30 cm	2.3 (1.0)^a	4.2 (1.2)^a	27.4 (9.0)^a

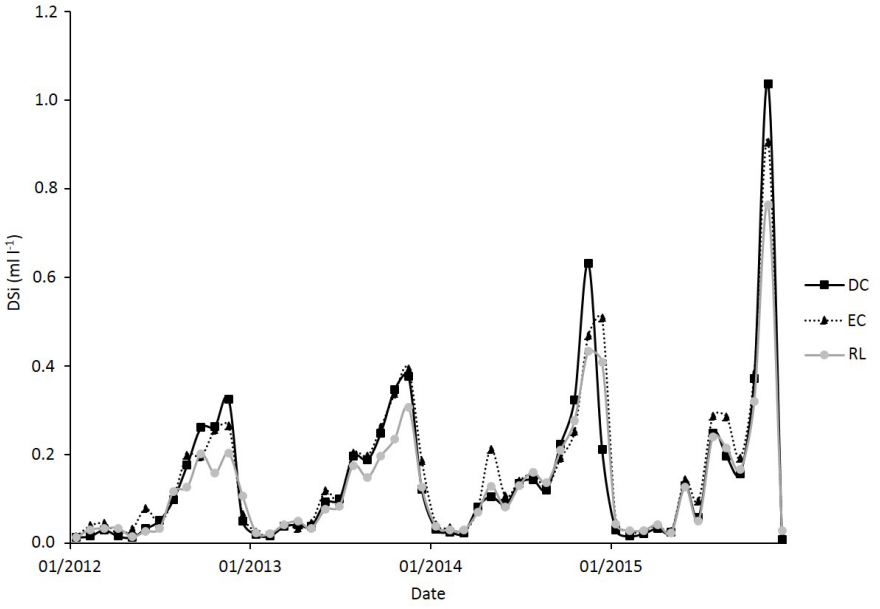

Figure 2. Seasonal dynamics over 4 years (January 2012 to December 2015) of DSi concentration in throughfall solution for the three plots, DC, EC and RL.

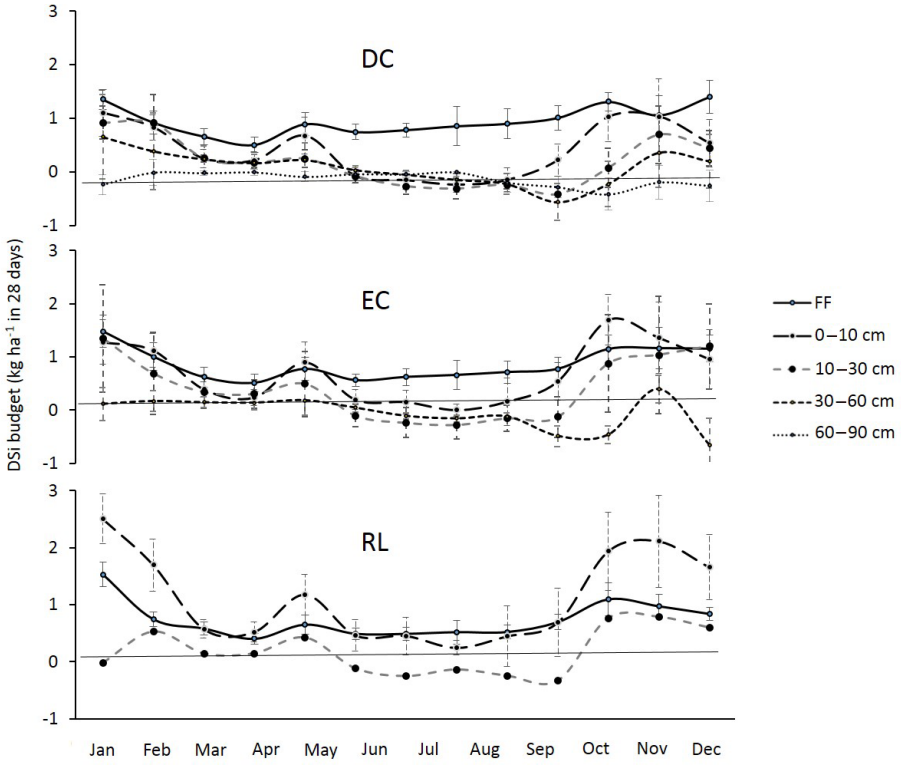

Figure 3. Seasonal dynamics over 4 years (January 2012 to December 2015) of the DSi budget in the different layers (forest floor, FF; soil 0–10 cm; soil 10–30 cm; soil 30–60 cm; and soil 60–90 cm) for the three plots, DC, EC and RL.

centration in this compartment (4.9 to 15.0 g kg^{-1}) but also from a large biomass. The Si content in fine beech roots was higher (2 to 6 times) than that measured by Maguire et al. (2017) for another deciduous species, i.e. sugar maple (*Acer saccharum*), but in a cooler environment. Besides Maguire et al. (2017) demonstrated in their study that in-

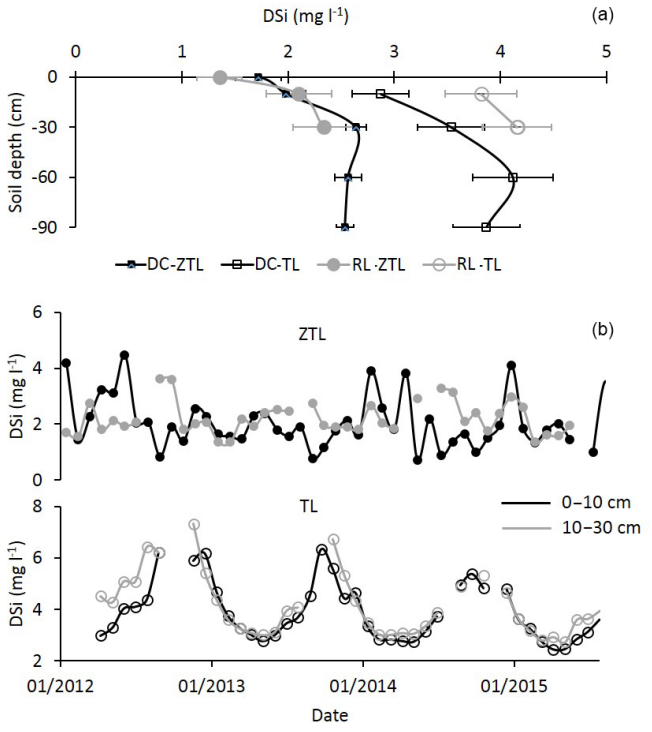

Figure 4. (a) Mean DSi concentration over 4 years (January 2012 to December 2015) in zero-tension lysimeters (ZTL) and tension lysimeters (TL) at different soil depths (0–10, 10–30, 30–60 and 60–90 cm) in plots DC and RL. For each soil type and depth, values with an asterisk are significantly different according to a Mann–Whitney U test at the threshold P value level of 0.05 (solution-type effect, ZTL vs. TL). **(b)** Seasonal dynamics over 4 years (January 2012 to December 2015) of DSi concentrations in ZTL and TL in the 0–10 cm and 10–30 cm soil layers of plot RL.

creased soil freezing significantly lowers the Si content of sugar maple fine roots. The fine beech root biomass ranged from 7.3 to 10.6 t ha^{-1} at the Montiers site. These values correspond to the upper part of the range of 2.4 to 9.6 t ha^{-1} reported in the literature for beech stands in Europe (Hendriks and Bianchi, 1995; Le Goff and Ottorini, 2001; Schmid, 2002; Claus and George, 2005; Bolte and Villanueva, 2006) and are in agreement with the fine-root biomass determined for another beech forest located in north-eastern France (7.4 to 9.8 t ha^{-1}; Bakker et al., 2008).

Because most of the Si accumulated in leaves and fine roots with rapid turnover (annual for leaves and estimated at 1.11 ± 0.21 y^{-1} for fine beech roots; Brunner et al., 2013), a large part of the Si taken up by trees returned to the soil each year via litterfall degradation (28 %, from 25.2 kg ha^{-1} in plot RL to 44.9 kg ha^{-1} in plot DC) and via the decomposition of fine-root necromass (approximately 71 %, from 67.9 kg ha^{-1} in plot RL to 109.5 kg ha^{-1} in plot DC) (Fig. 6, Table 2). As demonstrated by Sommer et al., 2013, only a small fraction (approximately 1 % in our study; from 1.0 kg ha^{-1} in plot RL to 1.8 kg ha^{-1} in plot DC) of the Si is taken up by the tree stand accumulated each year in the perennial tree compartments, i.e. the stem, branch and coarse roots (Fig. 6, Table 2). As a consequence, approximately 99 % of the Si taken up by the stand each year returned to the soil via recycling of fine roots and leaves. The Si that accumulated in the tree stand and returned to the soil (without considering the exploitation residuals) at the Montiers site ranged from 93 to 154 kg ha^{-1} yr^{-1}. This is higher than in other beech ecosystems previously studied, i.e. 20 kg ha^{-1} yr^{-1} (Cornelis et al., 2010a) and 34 kg ha^{-1} yr^{-1} (Sommer et al., 2013), mainly because the role of fine roots in the Si cycle was underestimated in previous studies. For example, Gérard et al. (2008), who modelled the cycle of Si in the soil of a temperate forest, estimated that the Si amount that accumulated in Douglas fir roots was less than 1 % of the total uptake.

4.2 Si residence time and budget in the forest floor

Because the amount of Si in the small wood was negligible in the three plots in comparison to that in the organic horizons (< 3 % of the Si contained in the forest floor), only the organic horizons will be discussed below.

4.2.1 Mineral soil content in organic horizons

Cornelis et al. (2010a) estimated that the proportion of soil with a moder humus type was approximately 40 % for a deciduous temperate forest. In our study, we determined that the fraction of soil mixed in the organic horizons, i.e. mull form, did not surpass 5 %. The higher rate of soil pollution in the study of Cornelis et al. (2010a) can be explained by the presence of a thick Oh layer in the moder that was in direct contact with the superficial soil layer and was characterized by an intense mixing of degraded organic matter with soil particles, induced by biological activities, mainly bioturbation by earthworms in these soils (Lavelle, 1988). The Si input by dust deposits in the organic horizons was negligible, with a maximum value of 6.0 kg ha^{-1} yr^{-1} (no stand interception) in comparison with a stock of 151 to 246 kg ha^{-1} of Si in the organic horizons. Lequy et al. (2014), who studied the mineralogy of the dust deposits at the Montiers site, observed that the Si deposits in throughfall were mainly quartz.

4.2.2 Si residence time in organic horizons

The main phytogenic Si input into the organic horizons was opal phytoliths (Krieger et al., 2017), which dissolve slowly (Fraysse et al., 2009) in comparison to the rate of organic matter mineralization. The residence time of Si in the organic horizons is higher than that of carbon (5.3 ± 0.8 vs. 1.9 ± 0.4 y). In addition, the presence of testate amoebae, organisms rich in Si (Fig. 1; Sommer et al., 2013), in the organic horizons suggests that a large part of the Si belonged to the protozoic Si pool. Sommer et al. (2013) estimated that testate amoebae may use half of the Si input by litterfall in

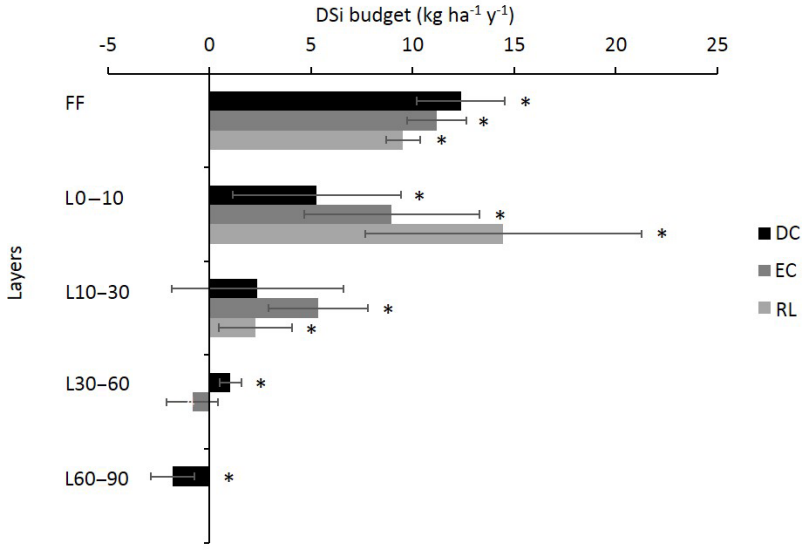

Figure 5. Mean annual DSi budget in the different layers (forest floor, FF; soil 0–10 cm; soil 10–30 cm; soil 30–60 cm; and soil 60–90 cm) for the three plots DC, EC and RL. Bars represent the SDs. Positive and negative values represent the production and immobilization of DSi in the given layer, respectively. Bars with an asterisk are significantly different from 0, according to a Mann–Whitney U test at the threshold P value level of 0.05.

beech organic horizons (17 vs. 34 kg ha^{-1}) for shell synthesis.

4.2.3 Si budget in organic horizons

During the study period (2012–2015), the Si input in the organic horizons via litterfall was primarily higher than the Si output via soluble transport (assessed in ZTL solutions under the forest floor) for the three soils. This net flux of Si should have induced the accumulation of Si in the organic horizons, which we did not observe in the 4 years of the study. This suggests the existence of another output flux which was not quantified in our study. This flux is likely the solid particulate migration toward the topsoil layer, as demonstrated by Ugolini et al. (1977). These authors observed that organic particles, notably containing silicon, were predominant in the migrant material in the upper soil layers. In our study, the solid particulate migration from the organic horizons to the topsoil may consist of the colloid transport of amoebae (Harter et al., 2000) or the transport of phytoliths (Fishkis et al., 2010). The latter observed, through a field study using fluorescent labelling, that the downward transport distance of phytoliths after 1 year was 3.99 ± 1.21 cm for a Cambisol with a preferential translocation of small-sized phytoliths.

4.3 Si budget and origin in soil

The Si production in the soil is mainly from pedogenic Si and BSi, resulting from soil mineral dissolution, and plant tissues and testate amoebae degradation, respectively (Cornelis et al., 2011; Sommer et al., 2013; Puppe et al., 2015). The immobilization (sink) of DSi in the soil is due to plant and organism accumulation and to the precipitation of secondary minerals, such as phyllosilicates or Si-bearing short-range organization minerals or allophane, immogolite (Dahlgren and Ugolini, 1989; Ma and Yamaji, 2006; Sommer et al., 2013; Tubana et al., 2016; Kabata-Pendias and Mukherjee, 2007).

Net production of DSi in the soils was observed on the three studied plots down to a depth of 60 cm, showing a positive production/immobilization budget. The net production of Si in the soil, ranging from 7.0 to 16.7 kg ha^{-1} yr^{-1}, was mainly located in the 0–10 cm layer, which probably accumulated amorphous Si from organic horizons that contained a large portion of fine roots from the soil. This is corroborated by the strong relationship between annual Si production in the 10–60 cm soil layers and fine-root content (data not shown, $r^2 = 0.94$). The contribution of fine roots to the production of DSi was higher in the superficial layer and decreased in the deep soil layers. A peak in net Si production was observed during autumn (except in the deeper soil layer; Fig. 3), which was probably due to an increase in Si production through the decomposition of dead roots. This finding is consistent with the studies of Meier and Leuschner (2008) and Konopka (2009), who demonstrated that fine-root necromass is highest at the end of the summer, when the soil is the driest, favouring root mortality. At our site, this period was also characterized by a maximum concentration of Si in the bound waters and a negative budget in the 10 to 60 cm soil layer, resulting from the precipitation of secondary minerals. As a result, a drastic decrease in Si production was observed in the surface layer during the vegetation period, where Si uptake by plants occurred (Fig. 3). In the deeper layer, the DSi budget was significantly negative and likely corresponded to

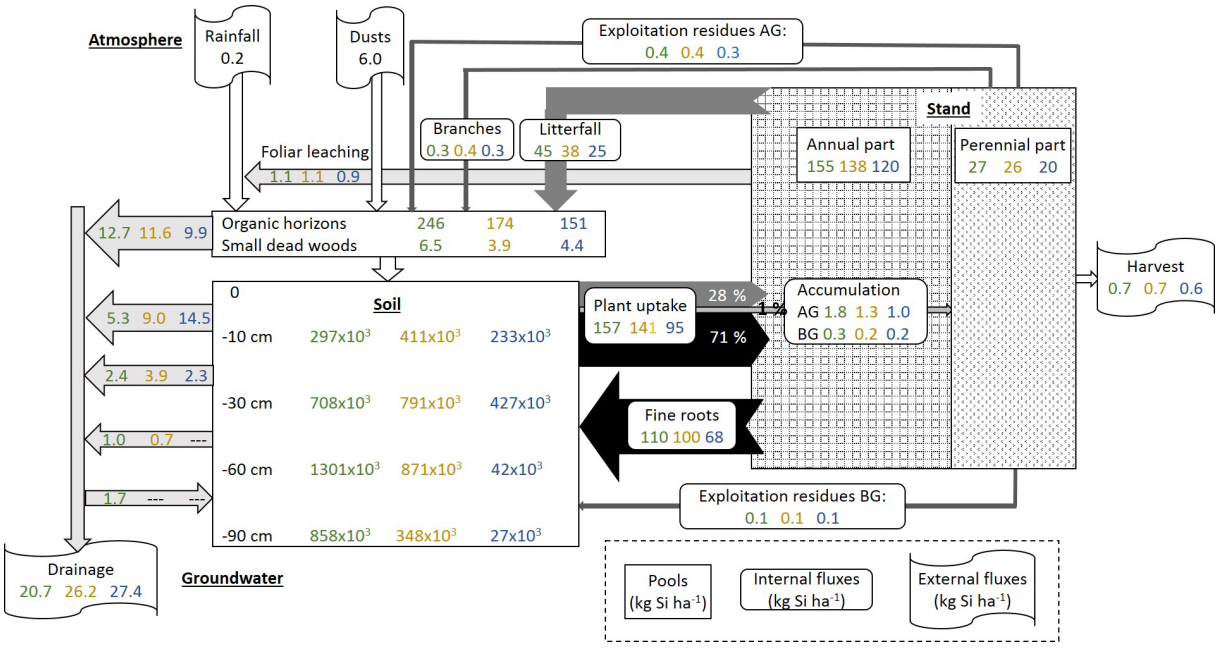

Figure 6. Summary scheme of Si cycling in plots DC, EC and RL at our study forest site, including (i) pools of Si in the biomass, (ii) internal Si fluxes, i.e. in the soil–plant system, (iii) external Si fluxes entering or leaving the soil–plant system and (iv) the DSi budget in the different layers of the ecosystem. Pools are presented by rectangular boxes (tree annual and perennial parts, organic horizons and small dead wood, and soil). Internal fluxes (solid form from the tree to the soil, i.e. fine roots, litterfall including leaves, buds and branches, and exploitation residues; and in solution from the soil to the plant, i.e. the tree uptake) are presented in boxes with rounded edges. Grey/black arrows indicate the direction and the intensity of the internal fluxes. The external fluxes (inputs: rainfall and dust deposits, and outputs: drainage and biomass harvest) are presented in flag boxes. For each pool and flux, values presented are those of the plots DC (in green), EC (in orange) and RL (in blue). The DSi budget in the different layers (forest floor and different soil layers) are represented with white arrows, which indicate the direction and the intensity of the fluxes. Arrows leaving the layer indicate the production of DSi in this layer. In contrast, arrows entering the layer indicate the immobilization of DSi in this layer. Values presented in each box and arrow are annual mean values for plots DC, EC and RL (except for atmosphere values which are similar for the three plots). The AG and BG correspond to above-ground and below-ground tree compartments.

mineral precipitation, induced by a decrease in Si drainage with depth, as observed by Sommer et al. (2013).

The Si produced in the soils was mainly leached out of the soil profile by drainage during winter. The annual drainage flux ranged from 21 to 27 kg Si ha^{-1} yr^{-1} in the three soils at the Montiers site, which is higher than those measured in other beech forests by Bartoli (1983; 0 kg Si ha^{-1} yr^{-1}), Cornelis et al. (2010b; 6 kg Si ha^{-1} yr^{-1}), Sommer et al. (2013; 14 kg Si ha^{-1} yr^{-1}) and Clymans et al. (2011; 18 kg Si ha^{-1} yr^{-1}). The differences can result from multiple factors, i.e. topography, soil properties (texture, structure, pH), rainfall (level and intensity) and other climatic factors, and stand characteristics (tree species and age, stem density, ground vegetal cover, etc.). In our study, the Si leached out of the soil profile was negligible compared to the Si taken up by trees, i.e. ratios of 1 : 4 and 1 : 7 in RL and DC. If we deduce the part of Si that was leached from the organic horizons, these ratios rise to about 1 : 5 and 1 : 22 in RL and DC. Because BSi in general is more soluble than lithogenic or pedogenic Si (Fraysse et al., 2009; Cornelis and Delvaux, 2016), very little of the Si leached within the soil profile directly results from the dissolution of soil minerals, as demonstrated in other studies in temperate forests (Bartoli, 1983; Watteau and Villemin, 2001; Gérard et al., 2008; Cornelis et al., 2010a, 2011; Sommer et al., 2006, 2013).

4.4 Si cycle at stand scale

Silicon inputs and outputs have minor contributions to the Si budget in our forest ecosystem, and the Si cycle is mainly driven by internal fluxes, especially recycling of BSi. However, Struyf et al. (2010) observed that land use is the most important controlling factor of Si mobilization in European watersheds. These authors showed that deforestation and conversion to agricultural land or other land uses lead to a 2-fold to 3-fold decrease in baseflow delivery of Si.

As explained above, the main part of the Si taken up by trees was allocated to annual compartments, i.e. 28 % to leaves, buds, beechnuts and fruit capsules and 71 % to fine roots (Fig. 6). Only 1 % of the Si taken up by trees was allocated to perennial tissues, i.e. stems, branches and coarse roots (Fig. 6). In addition, about half of the Si accumulated

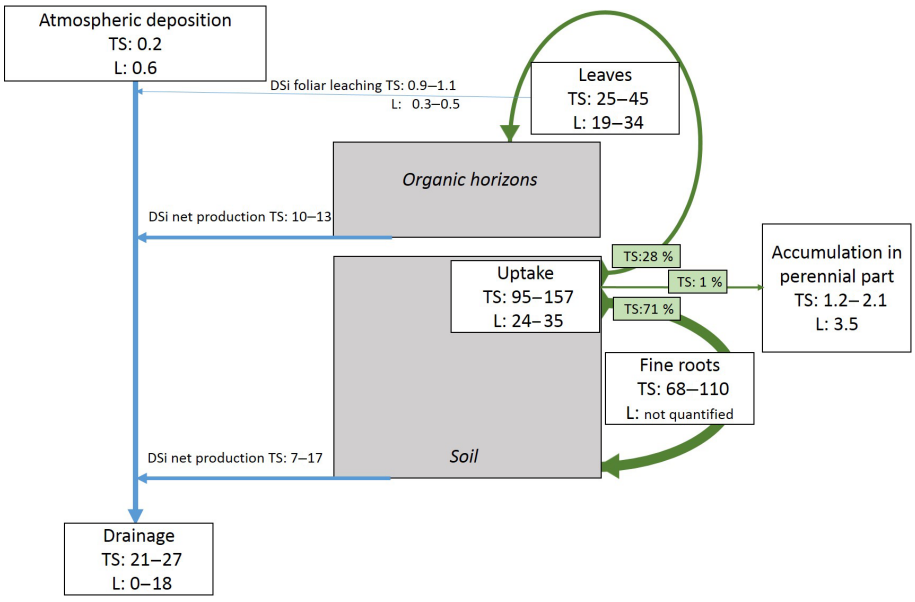

Figure 7. Summary scheme of the main findings of this study (TS) and comparison with other studies (L; Bartoli, 1983; Cornelis et al., 2010a; Sommer et al., 2013). The Si stocks and fluxes are in kg ha^{-1} of Si.

in the perennial tree compartments returned each year to the soil via branch falls and exploitation residues (< 7 cm diameter branches left on the floor and small/coarse roots left in the soil) and approximately 40 % was exported out of the site (stem and > 7 cm diameter branches). As a result, the amount of Si immobilized in trees remained almost constant over time at the stand scale (mean Si immobilization for the three plots, 0.1 kg ha^{-1} yr^{-1}).

In the organic horizons and in the soil, mainly in the 0–10 cm layer, we observed a high net Si production, likely resulting from the decomposition of litter leaves and testate amoebae in the organic horizons and of fine roots in the soil (Fig. 6). The seasonal dynamics of net Si production during the year suggests a relationship between biological activities and Si production, i.e. high net Si production at the end of the summer linked to fine-root decomposition and lower net Si production during spring/summer induced by tree uptake. Net Si production decreased with depth, and an immobilization of Si was observed in the deeper soil layer in plot DC (Fig. 6). This likely resulted from both a decrease in Si production (less root and clay) and the precipitation of Si through the formation of secondary minerals, resulting from reduced drainage flux.

The assessment of Si pools and fluxes in the different compartments of our forest ecosystem coupled with a seasonal dynamic follow-up reveal a rapid and almost total recycling of the Si at the stand scale and underline the key-role of biological processes, mainly fine roots, in the Si cycle.

4.5 Soil influence in the soil Si inputs/outputs

We showed that the Si content of plant compartments (leaves, organic horizons, above-ground and below-ground biomasses) was higher in the Si rich soils (plots DC and EC) compared to that of plot RL. This is in agreement with the observations of Heineman et al. (2016) in tropical forests, which demonstrated that nutrient concentrations in wood and leaves correlated positively with Ca, K, Mg and P concentrations in soils. The concentration of DSi in the soil is known to influence opal formation in plants (Cornelis et al., 2010b), but phytolith production seems to be more affected by the phylogenetic position of a plant than by environmental factors (Hodson et al., 2005). For example, these authors demonstrated through meta-analysis of the data, that in general ferns, gymnosperms and angiosperms accumulated less Si in their shoots than non-vascular plant species and horsetails. Moreover, the annual tree compartments (leaves and fine roots) were more concentrated in Si than the perennial compartments (branches, stem and coarse roots). Silicon plays several physiological and ecological functions in leaves and roots, such as involvement in the detoxification of aluminium, oxalic acid and heavy metals; in the regulation of ion balance; and in the reduction of hydric, salt and temperature stresses (Currie and Perry, 2007; Meunier et al., 2017). Silicon also contributes to the optimization of photosynthesis by gathering and scattering light in the leaves, conferring mechanical support and tissue rigidity, and facilitate pollen release, germination and tube growth (Bauer et al., 2011; Currie and Perry, 2007; Gal et al., 2012). In addition to these physiological functions, Si has also eco-

logical significance by protecting plants against herbivores and phytopathogens (Currie and Perry, 2007; Lins et al., 2002). The variations in Si content in the annual tree compartments induced by the soil type significantly affected the Si fluxes in the ecosystem. The annual uptake and Si recycling (leaves and buds, beechnuts, fruit capsules and fine roots) were 127.2 and 154.0 kg ha^{-1} in plot DC, as opposed to 94.8 and 92.7 kg ha^{-1} in plot RL.

In return, the bound solutions were more concentrated in Si in plot RL compared to in plot DC. This is partly due to the higher clay content in plot RL compared to in plot DC (clay was 2 times higher in plot RL). This considerably increases the specific surface area of minerals and improves their weatherability and water retention capacity (Carroll and Starkey, 1971; Petersen et al., 1996).

5 Conclusion

By coupling different approaches (annual budget in solid vegetal and solution phases and monthly dynamics of solutions) and methods (direct in situ measurements and standard and site-specific modelling) to quantify Si pools and fluxes in the different ecosystem compartments, our study allowed us to assess the Si cycle at the forest stand scale. Interestingly, our study highlights the main contribution of fine roots and, to a lesser extent, of leaves in the Si cycle (Fig. 7). Almost all the DSi was taken up by trees at any given time (very weak leaching out of the soil profile) and was recycled each year (approximately 99 %, only 1 % accumulated in perennial tissues). This suggests that the Si cycle is almost closed during the vegetation period: DSi is taken up by vegetation, then Si is returned to the soil mainly through root and leave decomposition in the form of DSi, which is again taken up by vegetation. This observation is consistent with that of Sommer et al. (2013), who demonstrated a low contribution of geochemical weathering processes to the Si cycle in a forest biogeosystem on a decadal timescale. The seasonal dynamics of DSi confirmed the key role of biological processes in the Si cycle, notably through the massive production of DSi during the decomposition of fine roots. Our study also revealed that soil type influences the Si accumulation in trees and the Si production in the soil. Trees accumulated more Si when developed on a Si-richer soil such as DC, resulting in higher Si recycling (factor of 1.6). While Si release was relatively similar in the organic horizons for the three plots, its production in the soil, mainly in the 0–10 cm layer, was twice as high in plot RL and richer in clays than in plot DC.

Further research is needed in the medium term (i) to assess the mineralization speed of fine roots in the soil and the speed of transformation of the root BSi into DSi; (ii) to determine the annual and seasonal fates of the DSi issued from roots between uptake, mineral precipitation, drainage and fixation by organisms; and (iii) to quantify the vertical transfer of solid particulates between organic horizons and topsoil.

Data availability. Some underlying data can be accessed in the Supplement (Figs. S1 and S2).

Supplement. The supplement related to this article is available online at: https://doi.org/10.5194/bg-15-2231-2018-supplement.

Competing interests. The authors declare that they have no conflict of interest.

Acknowledgements. We acknowledge Serge Didier for site implementation and management; Laurent Saint-André, Laura Franoux and Astrid Genêt for the development of allometric equations; Claire Pantigny, Louisette Gelhaye, Bruno Simon, Claude Nys, Jonathan Mangin, Céline Goldstein, Frédérique César, Maëlle D'Arbaumont and Maxime Simon for technical help; Lise Salsi, for preparing the samples and performing the SEM and EDX analyses; the National Forest Office (ONF) for welcoming our experimental site in the domanial forest of Montiers and for the stand management and American Journal Experts; and Krista Bateman for reviewing the English of the paper, as well as the reviewers who have, through their suggestions, significantly improved the quality of the manuscript. The authors acknowledge the facilities of the French National Institute for Agricultural Research and the Service d'Analyse des Roches et des Minéraux of the French National Center for Scientific Research. This work was supported by the Andra and INRA (accord spécifique no. 9) and GIP-Ecofor (contract no. 1138451B).

Edited by: Michael Bahn
Reviewed by: Eric Struyf and one anonymous referee

References

Alexandre, A., Meunier, J. D., Colin, F., and Koud, J. M.: Plant impact on the biogeochemical cycle of silicon and related weathering processes, Geochim. Cosmochim. Ac., 61, 677–682, 1997.

Alexandre, A., Bouvet, M., and Abbadie, L.: The role of savannas in the terrestrial Si cycle: a case study from Lamto, Ivory Coast, Global Planet. Change, 78, 162–169, 2011.

Bakker, M. R., Turpault, M. P., Huet, S., and Nys, C.: Root distribution of *Fagus sylvatica* in a chronosequence in western France, J. Forest Res., 13, 176–184, 2008.

Bartoli, F.: The biogeochemical cycle of silicon in two temperate forest ecosystems, Ecol. Bull., 35, 469–476, 1983.

Bartoli, F. and Souchier, B.: Cycle et rôle du silicium d'origine végétale dans les écosystèmes forestiers tempérés, Ann. Sci. Forest., 35, 187–202, 1978.

Bauer, P., Elbaum, R., and Weiss, I. M.: Calcium and silicon mineralization in land plants: transport, structure and function, Plant Sci., 180, 746–756, 2011.

Blecker, S. W., McCulley, R. L., Chadwick, O. A., and Kelly, E. F.: Biologic cycling of silica across a grassland bioclimosequence, Global Biogeochem. Cy., 20, 3023, https://doi.org/10.1029/2006GB002690, 2006.

Bolte, A. and Villanueva, I.: Interspecific competition impacts on the morphology and distribution of fine roots in European beech (*Fagus sylvatica* L.) and Norway spruce (*Picea abies* (L.) Karst.), Eur. J. For. Res., 125, 15–26, 2006.

Brunner, I., Bakker, M. R., Björk, R. G., Hirano, Y., Lukac, M., Aranda, X., Børja, I., Eldhuset, T. D., Helmisaari, H. S., Jourdan, C., Konôpka, B., Miguel Pérez, C., Persson, H., and Ostonen, I.: Fine-root turnover rates of European forests revisited: an analysis of data from sequential coring and ingrowth cores, Plant Soil, 362, 357–372, 2013.

Calvaruso, C., Kirchen, G., Saint-André L., Redon, P.-O., and Turpault, M.-P.: Relationship between soil nutritive resources and the growth and mineral nutrition of a beech (*Fagus sylvatica*) stand along a soil sequence, Catena, 155, 156–169, 2017.

Carroll, D. and Starkey, H. C.: Reactivity of clay minerals with acids and alkalies, Clay. Clay Miner., 19, 321–333, 1971.

Claus, A. and George, E.: Effect of stand age on fine-root biomass and biomass distribution in three European forest chronosequences, Can. J. Forest Res., 35, 1617–1625, 2005.

Clymans, W., Struyf, E., Govers, G., Vandevenne, F., and Conley, D. J.: Anthropogenic impact on amorphous silica pools in temperate soils, Biogeosciences, 8, 2281–2293, https://doi.org/10.5194/bg-8-2281-2011, 2011.

Conley, D. J.: Terrestrial ecosystems and the global biogeochemical silica cycle, Global Biogeochem. Cy., 16, 1–8, 2002.

Cornelis, J. T. and Delvaux, B.: Soil processes drive the biological silicon feedback loop, Funct. Ecol., 30, 1298–1310, 2016.

Cornelis, J. T., Ranger, J., Iserentant, A., and Delvaux, B.: Tree species impact the terrestrial cycle of silicon through various uptakes, Biogeochemistry, 97, 231–245, 2010a.

Cornelis, J. T., Delvaux, B., Cardinal, D., Andre, L., Ranger, J., and Opfergelt, S.: Tracing mechanisms controlling the release of dissolved silicon in forest soil solutions using Si isotopes and Ge/Si ratios, Geochim. Cosmochim. Ac., 74, 3913–3924, 2010b.

Cornelis, J. T., Titeux, H., Ranger, J., and Delvaux, B.: Identification and distribution of the readily soluble silicon pool in a temperate forest below three distinct tree species, Plant Soil, 342, 369–378, 2011.

Currie, H. A. and Perry, C. C.: Silica in plants: biological, biochemical and chemical studies, Ann. Bot.-London, 100, 1383–1389, 2007.

Dahlgren, R. A. and Ugolini, F. C.: Effects of tephra addition on soil processes of spodosols in the Cascade Range, Washington, USA, Geoderma, 45, 331–335, 1989.

Emsens, W. J., Schoelynck, J., Grootjans, A. P., Struyf, E., and Van Diggelen, R.: Eutrophication alters Si cycling and litter decomposition in wetlands, Biogeochemistry, 130, 289–299, 2016.

Epstein, E.: Silicon, Annu. Rev. Plant Phys., 50, 641–664, 1999.

FAO: World Reference Base for Soil Resources 2014, in: World Soil Resources Report 106, FAO, Rome, 1–192, 2016.

Finér, L., Ohashib, M., Noguchic, K., and Hiranod, Y.: Factors causing variation in fine root biomass in forest ecosystems, Forest Ecol. Mangag., 261, 265–277, 2011.

Fishkis, O., Ingwersen, J., Lamers, M., Denysenko, D., and Streck, T.: Phytolith transport in soil: a field study using fluorescent labelling, Geoderma, 157, 27–36, 2010.

Fraysse, F., Pokrovsky, O. S., Schott, J., and Meunier, J. D.: Surface chemistry and reactivity of plant phytoliths in aqueous solutions, Chem. Geol., 258, 197–206, 2009.

Gal, A., Brumfeld, V., Weiner, S., Addadi, L., and Oron, D.: Certain biominerals in leaves function as light scatterers, Adv. Mater., 24, 77–83, 2012.

Gaul, D., Hertel, D., and Leuschner, C.: Estimating fine root longevity in a temperate Norway spruce forest using three independent methods, Funct. Plant Biol., 36, 11–19, 2009.

Gérard, F., Mayer, K. U., Hodson, M. J., and Ranger, J.: Modelling the biogeochemical cycle of silicon in soils: application to a temperate forest ecosystem, Geochim. Cosmochim. Ac., 72, 741–758, 2008.

Granier, A., Bréda, N., Biron, P., and Villette, S.: A lumped water balance model to evaluate duration and intensity of drought constraints in forest stands, Ecol. Model., 116, 269–283, 1999.

Harter, T., Wagner, S., and Atwill, E. R.: Colloid transport and filtration of *Cryptosporidium parvum* in sandy soils and aquifer sediments, Environ. Sci. Technol., 34, 62–70, 2000.

Heineman, K. D., Turner, B. L., and Dalling, J. W.: Variation in wood nutrients along a tropical soil fertility gradient, New Phytol., 211, 440–454, 2016.

Hendriks, C. M. A. and Bianchi, F. J. J. A.: Root density and root biomass in pure and mixed forest stands of Douglas-fir and Beech, Neth. J. Agr. Sci., 43, 321–331, 1995.

Henry, M., Picard, N., Trotta, C., Manlay, R., Valentini, R., Bernoux, M., and Saint-André, L.: Estimating tree biomass of sub-Saharan African forests: a review of available allometric equations, Silva Fenn., 45, 477–569, 2011.

Hodson, M. J., White, P. J., Mead, A., and Broadley, M. R.: Phylogenetic variation in the silicon composition of plants, Ann. Bot.-London, 96, 1027–1046, 2005.

Jones, L. H. P. and Handreck, K. A.: Studies of silica in the oat plant. III. Uptake of silica from soils by plant, Plant Soil, 23, 79–96, 1965.

Jourdan, C., Silva, E. V., Goncalves, J. L. M., Ranger, J., Moreira, R. M., and Laclau, J. P.: Fine root production and turnover in Brazilian Eucalyptus plantations under contrasting nitrogen fertilization regimes, For. Ecol. Manage., 256, 396–404, 2008.

Kabata-Pendias, A. and Mukherjee, A. B.: Trace Elements from Soil to Human, Springer, Berlin, 2007.

Kirchen, G., Calvaruso, C., Granier, A., Redon, P.-O., Van Der Heijden, G., Bréda, N., and Turpault, M.-P.: Local soil type variability controls the water budget and stand productivity in a beech forest, Forest Ecol. Mangag., 390, 89–103, 2017.

Konôpka, B.: Differences in fine root traits between Norway spruce (*Picea abies* (L.) Karst.) and European beech (*Fagus sylvatica* L.) – a case study in the Kysucké Beskydy Mts, J. For. Sci., 55, 556–566, 2009.

Krieger, C., Calvaruso, C., Morlot, C., Uroz, S., Salsi, L., and Turpault, M.-P.: Identification, distribution, and quantification of biominerals in a deciduous forest, Geobiology, 15, 296–310, 2017.

Lavelle, P.: Earthworm activities and the soil system, Biol. Fert. Soils, 6, 237–251, 1988.

Le Goff, N. and Ottorini, J.-M.: Root biomass and biomass increment in a beech (*Fagus sylvatica* L.) stand in North-East France, Ann. For. Sci., 58, 1–13, 2001.

Legout, A., Legout, C., Nys, C., and Dambrine, E.: Preferential flow and slow convective chloride transport through the soil of a forested landscape (Fougères, France), Geoderma, 151, 179–190, 2009.

Lequy, E., Calvaruso, C., Conil, S., and Turpault, M.-P.: Atmospheric particulate deposition in temperate deciduous forest ecosystems: interactions with the canopy and nutrient inputs in two beech stands of Northeastern France, Sci. Total Environ., 487, 206–215, 2014.

Lins, U., Barros, C. F., da Cunha, M., and Miguens, F. C.: Structure, morphology, and composition of silicon biocomposites in the palm tree *Syagrus coronata* (Mart.), Becc., Protoplasma, 220, 89–96, 2002.

Lucas, Y., Luizao, F. J., Chauvel, A., Rouiller, J., and Nahon, D.: The relation between biological activity of the rain forest and mineral composition of soils, Science, 260, 521–523, 1993.

Ma, J. F. and Yamaji, N.: Silicon uptake and accumulation in higher plants, Trends Plant Sci., 11, 392–397, 2006.

Maguire, T. J., Templer, P. H., Battles, J. J., and Fulweiler, R. W.: Winter climate change and fine root biogenic silica in sugar maple trees (*Acer saccharum*): implications for silica in the Anthropocene, J. Geophys. Res.-Biogeo., 122, 708–715, 2017.

Meier, I. C. and Leuschner, C.: Belowground drought response of European beech: fine root biomass and carbon partitioning in 14 mature stands across a precipitation gradient, Glob. Change Biol., 14, 2081–2095, 2008.

Meunier, J. D., Barboni, D., Anwar-ul-Haq, M., Levard, C., Chaurand, P., Vidal, V., Grauby, O., Huc, R., Laffont-Schwob, I., Rabier, J., and Keller, C.: Effect of phytoliths for mitigating water stress in durum wheat, New Phytol., 215, 229–239, 2017.

Petersen, L. W., Moldrup, P., Jacobsen, O. H., and Rolston, D. E.: Relations between specific surface area and soil physical and chemical properties, Soil Sci., 161, 9–21, 1996.

Puppe, D., Kaczorek, D., Wanner, M., and Sommer, M.: Dynamics and drivers of the protozoic Si pool along a 10-year chronosequence of initial ecosystem states, Ecol. Eng., 70, 477–482, 2014.

Puppe, D., Ehrmann, O., Kaczorek, D., Wanner, M., and Sommer, M.: The protozoic Si pool in temperate forest ecosystems – quantification, abiotic controls and interactions with earthworms, Geoderma, 243, 196–204, 2015.

Puppe, D., Höhn, A., Kaczorek, D., Wanner, M., Wehrhan, M., and Sommer, M.: How big is the influence of biogenic silicon pools on short-term changes in water-soluble silicon in soils? Implications from a study of a 10-year-old soil–plant system, Biogeosciences, 14, 5239–5252, https://doi.org/10.5194/bg-14-5239-2017, 2017.

Richmond, K. E. and Sussman, M.: Got silicon? The non-essential beneficial plant nutrient, Curr. Opin. Plant Biol., 6, 268–272, 2003.

Saint-André, L., M'Bou, A. T., Mabiala, A., Mouvondy, W., Jourdan, C., Rouspard, O., Deleporte, P., Hamel, O., and Nouvellon, Y.: Age related equation for above and below ground biomass of a Eucalyptus in Congo, Forest Ecol. Manag., 205, 199–214, 2005.

Schmid, I.: The influence of soil type and interspecific competition on the fine root system of Norway spruce and European beech, Basic Appl. Ecol., 3, 339–346, 2002.

Sommer, M., Kaczorek, D., Kuzyakov, Y., and Breuer, J.: Silicon pools and fluxes in soils and landscapes – a review, J. Plant Nutr. Soil Sc., 169, 310–329, 2006.

Sommer, M., Jochheim, H., Höhn, A., Breuer, J., Zagorski, Z., Busse, J., Barkusky, D., Meier, K., Puppe, D., Wanner, M., and Kaczorek, D.: Si cycling in a forest biogeosystem – the importance of transient state biogenic Si pools, Biogeosciences, 10, 4991–5007, https://doi.org/10.5194/bg-10-4991-2013, 2013.

Struyf, E. and Conley, D. J.: Emerging understanding of the ecosystem silica filter, Biogeochemistry, 107, 9–18, 2012.

Struyf, E., Van Damme, S., Gribsholt, B., Bal, K., Beauchard, O., Middelburg, J. J., and Meire, P: Phragmites australis and silica cycling in tidal wetlands, Aquat. Bot., 87, 134–140, 2007.

Struyf, E., Smis, A., Van Damme, S., Garnier, J., Govers, G., Van Wesemael, B., Conley, D., Batelaan, O., Clymans, W., Vandevenne, F., Lancelot, C., Goos, P., and Meire, P.: Historical land use change has lowered terrestrial silica mobilization, Nat. Commun., 1, 129–135, 2010.

Tubana, B. S., Babu, T., and Datnoff, L. E.: A review of silicon in soils and plants and its role in us agriculture: history and future perspectives, Soil Sci., 181, 393–411, 2016.

Ugolini, F. C., Dawson, H., and Zachara, J.: Direct evidence of particle migration in the soil solution of a podzol, Science, 4317, 603–605, 1977.

Watteau, F. and Villemin, G.: Ultrastructural study of the biogeochemical cycle of silicon in the soil and litter of a temperate forest, Eur. J. Soil Sci., 52, 385–396, 2001.

White, A. F., Vivit, D. V., Schulz, M. S., Bullen, T. D., Evett, R. R., and Aagarwal, J.: Biogenic and pedogenic controls on Si distributions and cycling in grasslands of the Santa Cruz soil chronosequence, California, Geochim. Cosmochim. Ac., 94, 72–94, 2012.

Yuan, Z. H. and Chen, H. Y. H.: Fine root biomass, production, turnover rates, and nutrient contents in boreal forest ecosystems in relation to species, climate, fertility, and stand age: literature review and meta-analyses, Crit. Rev. Plant Sci., 29, 204–221, 2010.